Universidade de Aveiro
2021

Maria Silvina Marques Mendes

Pré-tratamento de fluidos humanos utilizando sistemas de partição em três fases para diagnóstico e prognóstico do cancro do pulmão

Human fluids pretreatment using three-phase partitioning systems for the diagnosis and prognosis of lung cancer

Universidade de Aveiro
2021

Maria Silvina Marques Mendes

Pré-tratamento de fluidos humanos utilizando sistemas de partição em três fases para diagnóstico e prognóstico do cancro do pulmão

Human fluids pretreatment using three-phase partitioning systems for the diagnosis and prognosis of lung cancer

Dissertação apresentada à Universidade de Aveiro para cumprimento dos requisitos necessários à obtenção do grau de Mestre em Bioquímica, realizada sob a orientação científica da Doutora Mara Guadalupe Freire Martins, Investigadora Coordenadora do CICECO – Instituto de Materiais de Aveiro, Departamento de Química, Universidade de Aveiro e coorientação da Doutora Ana Francisca Osório de Almeida Coelho e Silva, Investigadora Júnior do CICECO – Instituto de Materiais de Aveiro, Departamento de Química, Universidade de Aveiro.

Este trabalho foi desenvolvido no âmbito do projeto PTDC/EMD-TLM/3253/2020 (ILSurvive), financiado por fundos nacionais (OE), através da FCT/MCTES.

FCT
Fundação para a Ciência e a Tecnologia
MINISTÉRIO DA CIÊNCIA, TECNOLOGIA E ENSINO SUPERIOR

o júri

presidente

Prof. Doutora Rita Maria Pinho Ferreira
Professora Auxiliar da Universidade de Aveiro

Prof. Doutora Mara Guadalupe Freire Martins
Investigadora Coordenadora da Universidade de Aveiro

Prof. Doutora Fani Pereira de Sousa
Professora Associada da Universidade da Beira Interior

agradecimentos

A elaboração do presente trabalho não seria possível sem o apoio de alguns intervenientes. Assim sendo, pretendo agradecer a todos os que sempre me apoiaram e contribuíram para a realização e concretização desta etapa final do meu mestrado em Bioquímica.

Deste modo, agradeço:

À minha família, pois tudo isto foi possível graças ao esforço e dedicação que sempre tiveram. Por estarem sempre lá para me amparar e por todo o apoio incondicional.

À minha orientadora, a Drª Mara Freire, e coorientadora, a Drª Francisca Silva, pela oportunidade de realizar este trabalho e pelo acompanhamento ao longo do mesmo. Obrigada por me incentivarem a fazer sempre mais e melhor, e pelo enorme contributo que tiveram para o meu crescimento pessoal e educacional.

À Marguerita Rosa, por me ter acompanhado ao longo de todo este trabalho, por toda a atenção, compreensão e conhecimentos transmitidos. Obrigada pela paciência, pelas palavras amigas e pela ajuda incondicional.

Ao meu namorado que esteve sempre presente ao longo de todo este percurso e que sempre me apoiou de forma compreensiva e motivadora. Obrigada por todo o carinho, motivação e paciência.

Às minhas amigas que sempre estiveram presentes, com todo o apoio, carinho e compreensão.

palavras-chave

cancro do pulmão, pentraxina-3, depleção, sistemas aquosos bifásicos, sistemas de partição de três fases

resumo

A nível mundial, o cancro do pulmão apresenta a maior taxa de mortalidade associada a doenças oncológicas. A taxa de sobrevivência a 5 anos deste tipo de tumor é inferior a 15%, devido ao facto da maioria dos pacientes serem diagnosticados em fases avançadas. Assim, a deteção precoce do cancro do pulmão representa uma das abordagens mais promissoras para a redução da sua elevada mortalidade e morbidade. Os avanços tecnológicos nas áreas da genómica e da proteómica permitiram identificar novos biomarcadores que podem ser utilizados na deteção precoce de tumores. A pentraxina-3 (PTX3) é um destes biomarcadores, uma vez que a sua deteção e quantificação no soro humano permite o diagnóstico e prognóstico de cancro do pulmão. Porém, o soro humano é uma matriz muito complexa e cujo conteúdo proteico é constituído principalmente por albumina do soro humano (ASH) e imunoglobulina G (IgG). Estas proteínas podem interferir ou mesmo mascarar a deteção e quantificação de proteínas menos abundantes, tais como a PTX3, conduzindo a resultados falsos. De modo a possibilitar um diagnóstico precoce e mais fidedigno do cancro do pulmão, é necessário implementar etapas de pré-tratamento do soro humano que permitam a depleção das proteínas mais abundantes e simultânea concentração de biomarcadores tumorais. Neste contexto, os sistemas de partição em três fases à base de sistemas bifásicos aquosos (SAB) surgem como uma técnica alternativa às técnicas de pré-tratamento atuais que usam resinas de afinidade dispendiosas ou solventes orgânicos voláteis.

O objetivo principal deste trabalho é desenvolver novos sistemas de partição em três fases com base em SAB constituídos por polímeros/copolímeros e sais como estratégias alternativas de pré-tratamento de soro humano. Para tal, foram estudados novos sistemas compostos pelos homopolímeros PPG 400 e PEGs 400, 600, 1000 e 2000, e pelos copolímeros Pluronic PE6200, PE6400 e L35, e UCON, e tampão citrato, em termos da sua capacidade para simultaneamente precipitar a ASH e IgG na interfase e extrair o biomarcador PTX-3 para a fase rica em polímero. De acordo com os resultados obtidos, os sistemas formados por PPG 400, PEG 1000, PEG 2000 e UCON permitiram eficiências de depleção acima de 80% para ambas as proteínas, com os sistemas formados por PEG 1000 atingindo percentagens de depleção de 100% para as proteínas mais abundantes. Entre os melhores sistemas estudados, apenas o sistema com PEG 1000 permitiu a extração total da PTX-3 na fase rica em polímero, mantendo a depleção completa da IgG e HSA. Os ensaios de ELISA realizados mostraram a capacidade melhorada deste sistema para a quantificação de PTX-3 em amostras pré-tratadas, representando uma alternativa promissora para o pré-tratamento do soro humano no diagnóstico e prognóstico do cancro do pulmão.

keywords

lung cancer, pentraxin-3, depletion, aqueous biphasic systems, three-phase partitioning systems

abstract

Lung cancer is responsible for the highest rate of cancer mortality worldwide. The 5-year survival rate of lung cancer is less than 15%, mainly because most lung cancer patients are diagnosed at late stages. Therefore, early detection of lung cancer represents one of the most effective approaches to help reduce the high associated mortality and morbidity. Technological advances in genomics and proteomics fields have disclosed many novel cancer biomarkers, which can be used in early cancer detection. Pentraxin-3 is one of these promising biomarkers, found in serum, for lung cancer diagnosis and prognosis. However, human serum is a complex matrix whose protein profile mainly comprises human serum albumin (HSA) and immunoglobulin G (IgG). These proteins can interfere or even mask the detection and quantification of less abundant ones, such as PTX3, leading to false results. To contribute towards an earlier and more reliable diagnosis of lung cancer, there is a need to implement sample pretreatment steps that permit the depletion of the most abundant proteins and the concentration of tumor biomarkers of interest. In this context, three-phase partitioning (TPP) based on aqueous biphasic systems (ABS) are an alternative to conventional pretreatment techniques that use expensive affinity resins or volatile organic solvents.

The main goal of this work is to develop new TPP systems based on ABS composed of polymers/copolymers and salts as alternative serum pretreatment strategies. To this end, novel TPP-ABS formed by the homopolymers PPG 400, PEG 400, PEG 600, PEG 1000 and PEG 2000, and the copolymers Pluronic PE6200, Pluronic PE6400, Pluronic L35 and UCON, and a citrate buffered salt, were investigated in terms of their performance to simultaneous deplete HSA and IgG and extract the biomarker PTX-3 to the polymer-rich phase. According to the results obtained, TPP systems formed by PPG 400, PEG 1000, PEG 2000 and UCON allow depletion efficiencies above 80% for both proteins, with the systems formed by PEG 1000 and UCON allowing depletions efficiencies reaching 100% for both abundant proteins. Among the best studied systems, only the TPP system formed by PEG 1000 allows the complete extraction of PTX-3 towards the polymer-rich phase, while keeping the complete depletion of IgG and HSA. ELISA assays demonstrate the better performance of this TPP foe the PTX-3 quantification in the pretreated human serum samples, thus representing a promising alternative for the pretreatment of human serum for the diagnosis and prognosis of lung cancer.

CONTENTS

LIST OF FIGURES

LIST OF TABLES

LIST OF SYMBOLS AND ABBREVIATIONS

AA - Amino acids

ABS - Aqueous biphasic system

CEA - Carcinoembryonic antigen

CRP - C-reactive protein

DEX - Dextran

DCs - Dendritic cells

DE_{HSA}% - Depletion efficiency of HSA

DE_{IgG}% - Depletion efficiency of IgG

DE_{PTX-3}% - Depletion efficiency of PTX-3

DGNPs - Dextran-coated gold nanoparticles

DNA - Deoxyribonucleic acid

EC - Endothelial cells

ECM - Extracellular matrix

EE_{PTX-3}% - Extraction efficiency of PTX-3

EGFR - Epidermal growth factor receptor

ELISA - Enzyme-linked immunosorbent assay

GRP - Pro-gastrin-releasing peptide

GVHD - Graft-versus-host disease

HDL - High-density lipoproteins

HER2 - Human epidermal growth factor receptor 2

HGF - Hepatocyte growth factor

HSA - Human serum albumin

IARC - International Agency for Research on Cancer

IBP-1 - Insulin-like growth factor-binding protein 1

IgG – Immunoglobulin G

IL-1 - Interleukin-1

IL-6 - Interleukin 6

KRAS - Kirsten rat sarcoma viral oncogene homolog

LDH - Lactate dehydrogenase

LFA - Lateral-flow immunoassay

LLE - Liquid-liquid extraction

NSCLC - Non-small cell lung carcinoma

NSE - Neuron-specific enolase

NTA - Nanoparticle tracking analysis

PEG - Polyethylene glycol

PMNs - Polymorphonuclear cells

POC - Point-of-care

PSA - Prostate-specific antigen

PP - Protein precipitation

PTX3 - Pentraxin-3

RBP - Retinol-binding protein

RNA - Ribonucleic acid

SAP - Serum amyloid P

SCCA - Squamous cell carcinoma antigen

SCLC - Small cell lung carcinoma

SE-HPLC - Size Exclusion-High performance liquid chromatography

SERS - Surface enhanced Raman spectroscopy

SIA - Solvent interaction analysis

SPE - Solid phase extraction

SPR - Surface plasmon resonance

TL - Tie-line

TLL - Tie-line length

TLR - Toll-like receptors

TNFR1 - Tumor necrosis factor receptor 1

TPA - Tissue polypeptide antigen

TPP - Three-phase partitioning

TP53 - Tumor protein p53

TSG-14 - TNF-inducible gene 14 protein

WHO - World Health Organization

I - INTRODUCTION

1.1. GENERAL INTRODUCTION

According to the latest statistics available, lung cancer is the most common type of cancer and the leading cause of cancer mortality worldwide.[1] The number of deaths per year exceeds the total deaths caused by breast, colon and prostate cancer together.[1] The fundamental cause of such an high mortality is the diagnosis at later stages, often when cancer has become locally advanced and metastatic.[2]

Early detection of lung cancer, when a lesion is more responsive to treatment and more likely to be cured, represents one of the most promising approaches to reduce the mortality and morbidity associated.[3] The technological evolution of genomics and proteomics introduced many and novel cancer biomarkers, whose quantification in human fluids holds promise to be used as a tool for early cancer diagnosis.[4] These molecules play an increasingly important role in cancer staging and personalization of therapy at the time of diagnosis, improving the overall patient care.[5] Several proteins have been identified as potential lung cancer biomarkers, such as squamous cell carcinoma antigen (SCCA), neuron-specific enolase (NSE), cytokeratin 19 fragment (CYFRA 21-1) and, more recently pentraxin-3 (PTX3).[6,7] Nevertheless, biomarker detection remains a challenging task due to the complexity of biological samples, wide range of protein concentrations and labile nature of most protein-based biomarkers.[8] Since 80% of human serum proteins corresponds to human serum albumin (HSA) and immunoglobulin G (IgG),[9] these are very likely to interfere or even mask the detection of low-abundant proteins, including cancer biomarkers, leading to non-reliable diagnosis. To overcome this issue, it is necessary to implement sample pretreatment steps aiming the simultaneous depletion of high abundant serum proteins and the concentration of lung cancer biomarkers.[10]

The most used pretreatment techniques to reduce the content of HSA and IgG are liquid-liquid extraction (LLE),[11,12] solid phase extraction (SPE)[13,14] and protein precipitation (PP).[15,16] However, these techniques present some limitations. For example, LLE requires large amounts of organic solvents and may suffer from emulsion formation[17], whereas SPE exhibits limited selectivity and/or sensitivity and high cost associated to some of the most common protein-based affinity ligands used.[18] In turn, PP presents limited selectivity and may lead to biomarker losses.[19]

In the search for alternative techniques that could render sample pretreatment and biomarkers' concentration more cost-effective as well as bio- and eco-friendlier, aqueous

biphasic systems (ABS) can be foreseen as a viable option.[20] These are a class of liquid-liquid extraction systems mainly composed of water, comprising two water-rich phases of two incompatible solutes, such as two polymers, a polymer and a salt, or two salts.[21] ABS features have shown to be advantageous to extract cancer biomarkers from biological fluids, including prostate-specific antigen (PSA)[22] and extracellular vesicles (EVs),[23–25] both used in the diagnosis of prostate cancer. Also, it has been previously shown that when human serum is added to an ABS under certain conditions, proteins may partition between the aqueous phases or even precipitate at the interphase, forming a three-phase partitioning system (TPP).[26] Commonly, highly abundant serum proteins precipitate in the interphase of the ABS, while lower abundant ones [e.g., transferrin or lactate dehydrogenase (LDH)] are extracted into one of the ABS aqueous phases, allowing for posterior quantification.[26]

This work is focused on TPP/ABS pretreatment strategies to better identify and quantify the lung cancer biomarker PTX3 to improve the diagnosis of the deadliest oncologic disease worldwide. To this end, TPP/ABS composed of polymers/copolymers were investigated. Accordingly, this work faced the following stages:

(i) Determination of the ternary phase diagrams of ABS composed of several polymers/copolymers and citrate buffer using the cloud point titration method to define the mixture compositions needed to reach a biphasic regime;

(ii) Screening of ABS (or the corresponding TPP) to determine their ability to deplete high abundant proteins from commercial human serum by inducing their precipitation at the interphase;

(iii) Evaluation of the most efficient TPP to extract and concentrate PTX3 from spiked commercial human serum.

A schematic representation of the TPP-mediated sample pretreatment and lung cancer diagnosis proposed in the present MSc is given in Figure 1.1.

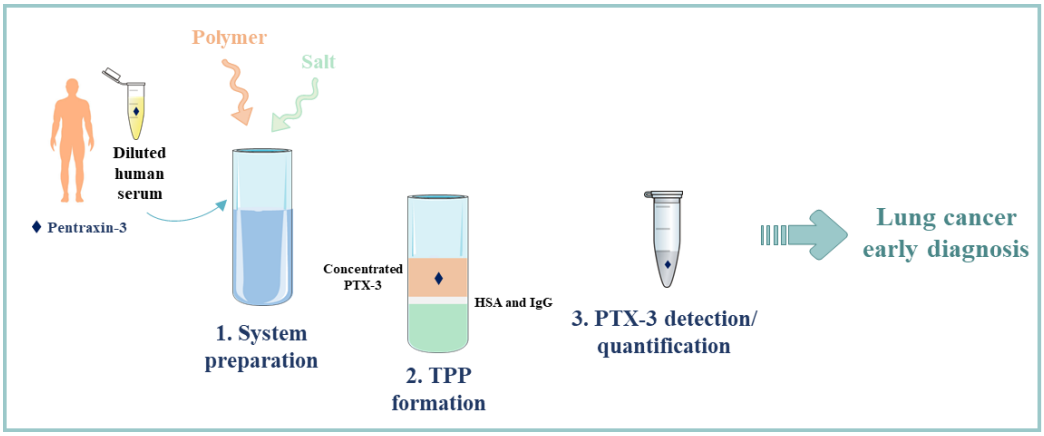

Figure 1.1. Schematic representation of the goal of this work.

Based on the exposed MSc objectives, this section provides an overview on cancer, in particular lung cancer, and its impact worldwide, diagnosis and prognosis. Particularly, the use of cancer biomarkers present in human serum as promising diagnosis and prognosis tools will be reviewed. Finally, an analysis of current serum pretreatment techniques will be performed and the application of ABS as an alternative technique for the extraction and concentration of disease biomarkers will be reviewed.

1.2. CANCER AND ITS GLOBAL IMPACT

Cancer represents a diversified class of diseases characterized by the uncontrolled growth and spread of abnormal cells. It is nowadays recognized as a major public health problem and the second cause of death globally.[27] The most frequent types of cancer in man are lung, prostate, colorectal, stomach and liver cancer, while breast, colorectal, lung, cervical and thyroid cancer prevail among women.[27]

Cancer incidence and mortality are growing worldwide.[28] The reasons for such an increase are complex, but contemplate both ageing and growth of the population, as well as changes in the distribution and prevalence of the main risk factors for cancer, including tobacco smoking and physical inactivity.[28] According to the latest statistics published by the International Agency for Research on Cancer (IARC) using the GLOBOCAN 2018, 18.1 million new cancer cases and 9.6 million cancer deaths worldwide were estimated to occur in 2018.[1] For both genders combined, it was estimated that approximately one-half of the cases and over one-half of the cancer deaths in the world took place in Asia.[1] Europe accounts for 23.4% of the total cancer cases and 20.3% of the cancer deaths, followed by America with 21% of incidence and 14.4% of mortality.[1] Lung cancer is the most diagnosed type of cancer (11.6% of the total cases) and the leading cause of cancer

death (18.4% of the total cancer deaths).[1,27] This is followed by female breast cancer (11.6%), colorectal cancer (10.2%), and prostate cancer (7.1%) for incidence and colorectal cancer (9.2%), stomach cancer (8.2%), and liver cancer (8.2%) for mortality.[1,27] Considering cancer incidence and mortality by sex, lung cancer is the most diagnosed cancer and the leading cause of cancer death in males, followed by prostate and colorectal cancer for incidence, and liver and stomach cancer for mortality.[1] Among females, breast cancer is the most commonly diagnosed cancer and the leading cause of cancer death, followed by colorectal and lung cancer for incidence, and vice versa for mortality.[1] For both sexes combined, lung cancer is the most commonly diagnosed cancer and the leading cause of cancer death, followed by female breast cancer, colorectal cancer, and prostate cancer for incidence and colorectal cancer, stomach cancer, and liver cancer for mortality,[1] as illustrated in Figure 1.2.

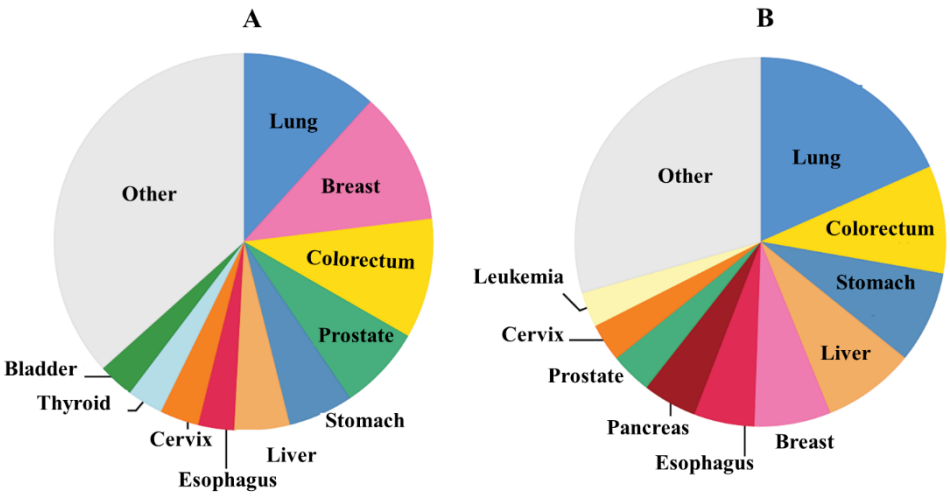

Figure 1.2. Distribution of incidence (A) and mortality (B) worldwide for the most common types of cancer observed in 2018 for men and women combined (adapted from [1]).

The cancer burden is growing globally, having significant physical, emotional, and financial impacts on individuals, families, communities and healthcare systems.[29] In 2008, the total economic impact of premature death and disability from cancer worldwide was about 895 billion dollars.[30] The lost years of life and productivity caused by cancer represent the largest drain on the global economy, compared to other causes of death.[31] Death and disability from lung, colon/rectal and breast cancers represent the largest economic costs on a global scale.[30] In low-income countries, cancers of the mouth and throat, cervix, and breast have the greatest impact.[30] Many health systems in low- and

middle-income countries are least prepared to manage this burden, and large numbers of cancer patients do not have access to timely and quality diagnosis and treatment.[30] In countries where healthcare systems are better organized and equipped, survival rates of many types of cancers are improving mostly due to the accessible early detection and adequate treatment.[30]

Carcinogenesis or tumorigenesis arise from multiple processes that drive normal cells to evolve progressively toward a malignant, neoplastic state, and ultimately to acquire metastatic features.[32] During this transformation, normal cells develop several capabilities that allow them to become carcinogenic and malignant. These biological capabilities that enable tumor growth and metastatic dissemination were initially categorized into six distinctive principles, proposed as the hallmarks of cancer by Hanahan and Weinberg[33]. The hallmarks of cancer are illustrated in Figure 1.3, which include sustaining proliferative signaling, evading growth suppressors, resisting cell death, enabling replicative immortality, inducing angiogenesis, and activating invasion and metastasis. In 2011, the same authors made new observations that led them to include the cancer cells ability to reprogram metabolism and to evade immune destruction to the list of the hallmarks of cancer.[34]

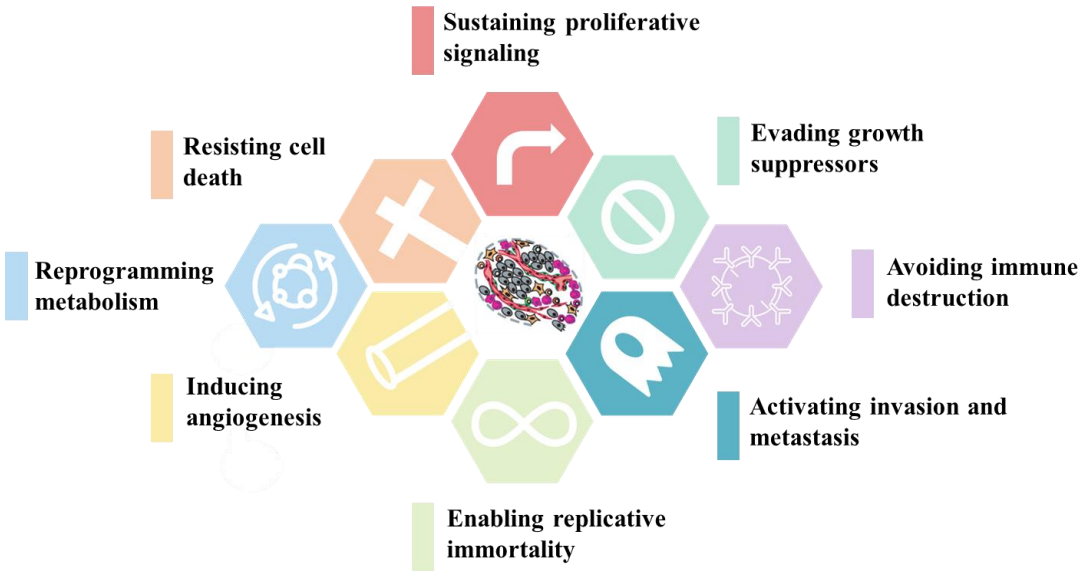

Figure 1.3. The Hallmarks of Cancer (adapted from [33]).

The most important feature of cancer cells is their capacity of sustaining chronic proliferation due to the inactivation of tumor suppressor genes.[33] The most common tumor suppressor genes encode for proteins such as tumor protein p53 (TP53) and

retinoblastoma-associated proteins that regulate cell proliferation and senescence programs.[33,35] The hallmark of resisting cell death is based on the capacity of cancer cells to resist death by apoptosis.[36,37] During tumorigenesis, apoptosis is triggered in response to several physiologic stresses, such as elevated levels of oncogenes and deoxyribonucleic acid (DNA) damage associated with hyperproliferation.[36] However, tumor cells developed a variety of strategies to circumvent apoptosis. The most common strategy is the loss of TP53 tumor suppressor function, eliminating this damage sensor from the apoptosis-inducing circuitry.[33] Tumors may also reach similar ends through the increase expression of antiapoptotic regulators or through the downregulation of proapoptotic factors.[33,36] The third hallmark is the enabling replicative immortality. Cancer cells require unlimited replicative potential to generate macroscopic tumors, unlike normal cell lineages, which are only able to go through a limited number of successive cell growth and division cycles. There are two distinct barriers to cell proliferation, which include senescence, an irreversible entrance into a non-proliferative but viable state, and crisis, that involves cell death.[33] The induction of angiogenesis is another important hallmark of cancer. Nevertheless, angiogenesis requires cells sustenance in form of nutrients and oxygen as well as an ability to excrete metabolic wastes and carbon dioxide, needs addressed by the tumor-associated neovasculature.[33,38] The sixth hallmark is characterized by the local invasion and distant metastasis resulting in the cancer progression to higher pathological grades of malignancy.[33] The associated cancer cells typically develop alterations in their shape as well as in their attachment to other cells and to the extracellular matrix (ECM). The process of invasion and metastasis is characterized by a sequence of multiple steps, often entitled the invasion-metastasis cascade.[39,40] This process starts with a succession of changes in normal cells, that allow the invasion by cancer cells into blood and lymphatic vessels, ending with the growth of micro metastatic lesions into macroscopic tumors.[39] The uncontrolled cell proliferation characteristic of this neoplastic disease involves not only deregulated control of cell proliferation but also corresponding adjustments of energy metabolism in order to fuel cell growth and division. The immune system plays an important role in the resistance or eradication of cancer cells.[34] The theory of immune surveillance proposes that cells are constantly checked by an ever-alert immune system, that recognizes and eliminates most of the cancer cells.[41] However, solid tumors have somehow managed to avoid the immune system detection, thereby evading eradication. Consequently, this tumor capability to escape the immune system detection plays an important role in tumor formation and progression.[34]

Nonetheless, tumor pathogenesis is complex and requires a repertoire of normal cells, molecules, and blood vessels to form tumor-associated stroma, contributing to the development and expression of the hallmark capabilities listed above.[34]

1.2.1. LUNG CANCER

Lung cancer is a highly invasive and rapidly metastasizing cancer and, as already mentioned, the primary cause of cancer-related deaths around the world.[1] In 2018, 2.1 million new lung cancer cases and 1.8 million deaths were estimated, representing about 18.4% of cancer deaths worldwide.[1] Among males, lung cancer is the leading cause of death in most countries in Eastern Europe, Western Asia, Northern Africa, and specific countries in Eastern Asia and South-Eastern Asia.[1] Among women, lung cancer is the deadliest within 28 countries.[1,27] The highest incidence rates are observed in Northern and Western Europe, North America, and Australia/New Zealand. In China, the incidence rates are like those observed in some Western European countries, notwithstanding substantial differences in smoking prevalence between the two populations. However, in Africa, the incidence rates persist generally low for both genders.[1,42] Lung cancer mortality in females has been lower than in men, but has been increasing in recent years in most countries. Differences in lung cancer incidence and mortality are associated with different patterns of smoking prevalence in different countries, since tobacco consumption is the main cause of all major histological types of lung cancer.[43] The excess risk among continuous smokers and never-smokers is in the order of 20 to 50 fold, being the duration of tobacco consumption considered the strongest determinant of lung cancer risk in smokers.[44,45] Other risk factors associated to lung cancer are genetic susceptibility (family history and high penetrance genes),[46] air pollution,[47] ionizing radiation,[48] occupational exposures,[49] poor diet[50] and chronic inflammation from infections and other medical conditions.[51–53] The previously referred risk factors may act independently or cooperatively with tobacco smoking in shaping the descriptive epidemiology of lung cancer.

Lung cancer poses a significant economic burden, being responsible for the highest estimated cost of all cancers.[54] In Europe, the overall economic impact of lung cancer is considerable, with direct costs such as costs of hospital and primary care, together with the costs of drugs, exceeding 3 billion euros annually.[55] When costs related with premature mortality and disability are added to direct costs, the annual cost of lung cancer surpasses 100 billion euros.[55] Based on these cost patterns, prevention and early detection

strategies are urgent to make lung cancer treatment more cost-effective, and potentially cost-saving.

Lung cancer arises from the cells of the respiratory epithelium and can be categorized into two main histological groups as illustrated in Figure 1.4. This categorization is based on the size and appearance of the malignant cells and includes small cell (SCLC) and non–small cell lung carcinoma (NSCLC).[56] SCLC represents about 15% of all lung cancer cases and is defined as a highly malignant tumor derived from cells exhibiting neuroendocrine characteristics. NSCLC accounts for the remaining 85% of cases and is subcategorized into adenocarcinomas, squamous cell carcinomas, large cell carcinomas.[57]

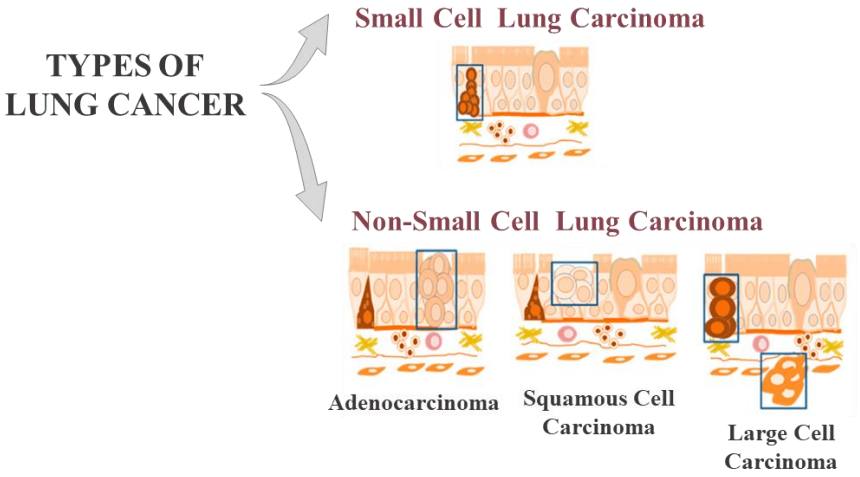

Figure 1.4. The World Health Organization (WHO) classification of lung cancer histological types. (Adapted from [58])

About 38.5% of all lung cancer cases are adenocarcinomas, with squamous cell carcinomas representing 20% and large cell carcinomas accounting for 2.9%.[59] Adenocarcinomas emerge from glandular cells of bronchial mucosa and represent the dominant histological subtype of lung cancer.[59,60] Squamous lung cancer arises from the modified bronchial epithelial cells and is characterized by some specific differentiation features, such as the presence of intercellular bridges, keratinization and keratin pearl formation. The subtype large cell carcinoma has its origin from epithelial cells of the lung and consists in a heterogenous group of undifferentiated malignant neoplasms that lack the cytologic and architectural features of small cell carcinoma and glandular or squamous differentiation.[59,60]

There are several exogenous and endogenous factors that influence the occurrence and development of lung cancer in each individual.[32] Thus, besides the various histological types, lung cancer also has many molecular and pathological subtypes characterized by heterogeneous cellular genetic and epigenetic changes, particularly activation of growth promoting pathways and inhibition of tumor suppressor pathways.[61] The lung tumorigenesis is related with the activation of growth promoting proteins, such as Kirsten rat sarcoma viral oncogene homolog (KRAS), epidermal growth factor receptor (EGFR), and human epidermal growth factor receptor 2 (HER2), as well as with the inactivation of tumor suppressor genes such as TP53. On the other hand, activation of growth promoting oncogenes can occur by gene amplification or other genetic alterations including point mutations and structural rearrangements, leading to uncontrolled signaling through oncogenic pathways.[61,62] Lung cancer survival depends on the histology and stage of the disease at diagnosis; therefore, the identification of the correct histological type of lung cancer and molecular subtypes is crucial to the development of an appropriate treatment strategy.[63]

1.3. DIAGNOSIS AND PROGNOSIS

The overall 5-year survival rate of lung cancer is less than 15%, mainly because most lung cancer patients are diagnosed at late stages, often when the cancer has become locally advanced and metastatic.[2] Currently, the diagnosis of lung cancer is primarily based on symptoms such as coughing, coughing up blood, chest pain and shortness of breath. The most commonly used methods for lung cancer diagnosis are chest radiography and computer tomography.[58,64] However, they can only identify visible and irreversible changes in lung, which occur in advanced stages and often when curative intervention is no longer effective. Thus, early diagnosis of lung cancer is the ideal approach to improve the survival chances of patients, while contributing to reduce the burden of the disease.[3] Remarkably, technological advances in genomics and proteomics have disclosed many promising biomarkers that can be used as tools for the early detection of multiple oncologic diseases, including lung cancer.[4]

1.3.1. CANCER BIOMARKERS

Biomarkers are biological molecules found in human body fluids, mostly blood, or tissues that can be objectively measured and evaluated as an indicator of a normal or abnormal biological process, or of a condition or disease, such as cancer.[65] As shown in Figure 1.5, tumor biomarkers can be epigenetic (changes in DNA methylation profile), genetic (mutations and changes in number of copies), proteomic (changes in level and profile of protein expression), metabolic (changes in level and spectrum of metabolites), DNAs and ribonucleic acids (RNAs), circulating tumor cells and protein biomarkers.[66–74]

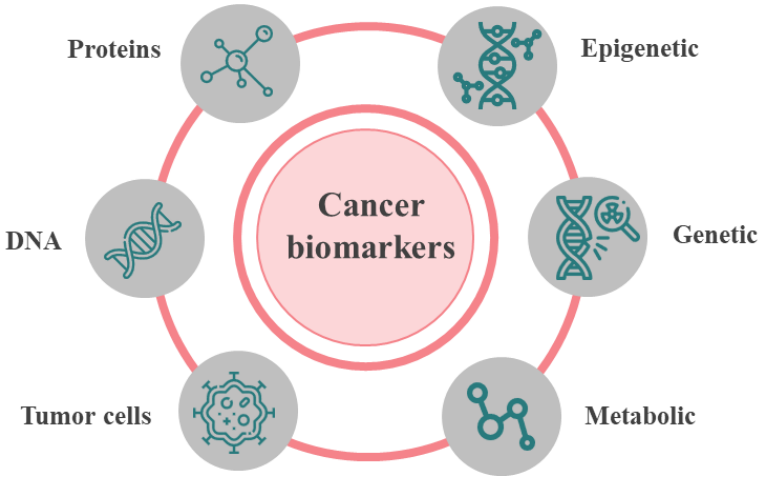

Figure 1.5. Types of cancer biomarkers.

Beyond early diagnosis, biomarkers can contribute for patient assessment in other clinical settings, namely in risk profiling, prognosis, and to guide decision-making related with treatment.[5] Based on their usage, cancer biomarkers can be classified into predictive, prognostic, and diagnostic biomarkers.[75] A predictive biomarker indicates the most likely benefit to the patient from specific therapeutic interventions. An example of a predictive biomarker is the gene HER2, whose activation predicts the patient response to trastuzumab in the case of breast cancer;[76–78] also, expression of the gene encoding the estrogen receptor predicts the response to the treatment with tamoxifen instead.[79] Considering the prognostic biomarkers, these provide information on the likely patient health outcome, such as cancer recurrence or disease progression in the future. For example, HER2/neu-positive breast tumors are more aggressive and have a worse prognosis compared to HER2/neu-negative tumors.[80] In turn, diagnostic biomarkers are used to identify whether a patient has a specific disease condition. For example, prostate-

specific antigen (PSA) is a widely used diagnostic biomarker whose levels are higher in patients with prostate cancer.[81]

Since most protein-based biomarkers are labile molecules and are present in low concentrations in complex biological fluids or tissues, the main challenge behind their use for cancer diagnosis remains the lack of reliability of the analysis procedures, leading frequently to false positive or false negative results.[8] Due to the low detection limits often imposed, current techniques require laborious and lengthy protocols, highly qualified workers, centralized laboratories and/or expensive specific reagents.[82] Most used techniques to detect and quantify cancer biomarkers in human body fluids comprise gel electrophoresis,[83,84] enzyme-linked immunosorbent assay (ELISA),[85] surface plasmon resonance (SPR),[86,87] surface enhanced Raman spectroscopy (SERS), [88,89] mass-sensing BioCD protein array, [90] fluorescence methods, [91,92] and calorimetric [93,94] and chemical assays.[95,96] As expected, the technique used for biomarker detection depends on the type of molecule to be quantified and on the source of the biomarker (e.g., urine, blood, sputum, etc.). For protein biomarkers the most commonly used method is ELISA.[97]

Several protein biomarkers are currently reported for the diagnosis and prognosis of lung cancer. Some examples are provided in Table 1. Carcinoembryonic antigen (CEA), squamous cell carcinoma antigen (SCCA), neuron-specific enolase (NSE), and CYFRA 21-1 are commonly used in clinical practice for lung cancer diagnosis and prognosis,[98] whereas insulin-like growth factor-binding protein 1 (IBP-1), lactate dehydrogenase (LDH), retinol-binding proteins (RBP) and pro-gastrin-releasing peptide (GRP) were only identified as promising lung cancer biomarkers.[99–102] More recently, the soluble pattern recognition receptor long pentraxin-3 (PTX3) has been proposed as a promising lung cancer biomarker allowing an early diagnosis.[7] Besides, this protein has shown to be an useful prognostic marker for lung carcinoma patients.[103]

Table 1.1. Examples of lung cancer protein biomarkers, biological fluid in which they are present, and cut-off value. (ND = Not determined)

Protein biomarker	Biological fluid	Cut-off value	Reference
CEA	Blood	>5 ng/mL	104–106
CYFRA21-1	Blood	>5.6 ng/mL	105,107
IBP-1	Urine	ND	99
LDH	Blood	>250 U/L	100,108
NSE	Blood	>15.45 ng/mL	109,110
RBP	Blood	ND	101,106

SCCA	Blood	>2.6 ng/mL	[106,111]
PTX3	Blood	>4.5 ng/mL	[7]
GRP	Blood	>0.066 pg/mL	[102,112]

1.3.1.1.PENTRAXIN-3 (PTX-3)

Pentraxins constitute a superfamily of proteins that share the same domain and are arranged in a cyclic pentameric structure.[113,114] The pentraxin domain consists of a 205 amino acids (AA) long conserved sequence located in their carboxy-terminal with a similar eight AA (His-x-Cys-x-Ser/Thr-Trp-x-Ser, in which x represent any AA) sequence called the pentraxin signature.[115] Based on the length of the protein sequence, the pentraxin family can be divided into short and long pentraxins. C-reactive protein (CRP) and serum amyloid P (SAP) are prototypical short pentraxins with approximately 25 kDa, whereas PTX3 is a 45 kDa protein that serves as prototype of the long pentraxin subfamily.[115,116]

PTX3, also known as TNF-inducible gene 14 protein (TSG-14), was first identified in the early 1990s in endothelial cells and fibroblasts.[117] The prototypic long PTX3 has a carboxy-terminal sharing a high degree of homology with short pentraxins coupled to an unrelated amino-terminal region. Despite of the sequence homology, PTX3 differ from short pentraxins in terms of gene organization, chromosomal localization, as well as cellular source, inducing-stimuli, and ligand-binding properties.[118,119]

The human PTX3 gene is located on chromosome 3q25 and has three exons separated by two introns.[117] The two first two exons code for the leader peptide and the amino-terminal domain (amino acids 18-178) of the protein, respectively, and the third exon encodes the carboxy-terminal pentraxin domain (amino acids 179-381).[117]

The PTX3 expression occurs in response to a variety of inflammatory or infectious stimuli. This protein interacts with different ligands such as microbial moieties, complement components and extracellular matrix components.[120,121] In contrast with short pentraxins, produced in the liver in response to interleukin 6 (IL-6), PTX3 is rapidly produced and released by a variety of different cells.[118] PTX3 was first identified as an early induced gene in monocytes and vascular endothelial cells (ECs).[117] Myeloid dendritic cells (DCs) and peripheral blood leukocytes also express significant levels of PTX3 in response to proinflammatory cytokines, agonists of toll-like receptors (TLR) or following stimulation with microbial components, including lipopolysaccharide, lipoarabinomannan, and outer cell membrane proteins.[118–120] PTX3 production is also

stimulated by the anti-inflammatory cytokine interleukin-10 (IL-10) and by high-density lipoproteins (HDLs).[122,123] More recently, renal and alveolar epithelial cells have also been found to produce lower amounts of PTX3 under stimulation.[124,125] Furthermore, the presence of PTX3 was observed in specific lactoferrin-positive granules of human neutrophils by intracellular labeling.[126] Other cell types can produce PTX3 in response to appropriate proinflammatory stimulation such as endothelial cells, smooth muscle cells, adipocytes, synovial cells, chondrocytes and fibroblasts.[123,127–130]

PTX3 behaves as an acute phase response protein considering that its blood levels are lower in normal conditions (<2 ng/ml), and rise quickly during inflammatory and infectious conditions such as endotoxic shock and sepsis, correlating with the severity of the disease.[131] Inflammation is considered an essential component of tumor microenvironment that affects tumor development and growth,[132] and since PTX3 is expressed in inflammatory conditions, this protein has been reported as a local or systemic marker of cancer-related inflammation. Elevated expression of PTX3 has been observed in pancreatic carcinoma,[133] gastric cancer,[134] myeloproliferative neoplasms,[135] lung cancer,[7,136,137] gliomas[138] and soft tissue liposarcoma.[139] In cervical cancer, PTX3 expression has been associated with tumor grade and differentiation, and in pancreatic carcinoma, higher PTX3 levels were associated with advanced clinical stage and poor overall survival.[133,140]

The high levels of PTX3 in serum of lung cancer patients are not totally understood. Due to known overexpression by macrophages and endothelial cells in response to inflammation, it is suggested that PTX3 may act as a biomarker for lung carcinoma, in response to the inflammatory microenvironment of the tumor.[141] In the last decade several studies have reported the role of PTX3 as a biomarker in lung cancer. Planque et al.[136] performed a proteomic based analysis of several lung cancer cell lines of differing histotypes and reported that lung cancer cells produce PTX3. This observation was confirmed in patients with lung cancer, in which PTX3 plasma levels were significantly higher compared with healthy subjects.[137] Serum PTX3 concentrations of > 4.5 ng/mL are considered abnormal and used as a cutoff value. Moreover, PTX3 circulating concentrations positively correlated with tumor stage and disease aggressiveness.[7] Indeed, high expression of PTX3 was associated with worse overall survival in small and non-small-cell lung carcinoma, being a negative prognostic indicator in these pathologies.[103,137] Besides human plasma or serum, PTX3 can also be found in other biological fluids such as urine,[142] pleural,[143] cerebrospinal fluid,[144] joint fluid[145] and

amniotic fluid.[146] However, the number of reports investigating the value of PTX3 in body fluids, other than plasma or serum, is very limited.

1.4. HUMAN SERUM PRETREATMENT TECHNIQUES

Body fluids, such as human serum, are very complex matrices containing miscellaneous components, including cells, proteins and other lower abundance molecules.[8] As previously discussed, the major technical challenge in the analysis of serum proteome is that their proteins are present at unequal concentrations and are quite labile.[9] Human serum albumin (HSA) and immunoglobulin G (IgG) represent almost 80% of total protein weight in human serum, which interfere or even mask the detection of other proteins, especially low abundant ones with clinical relevance, such as cancer biomarkers that represent less than 1% of the blood molecules, and in some cases may exist in attomolar concentrations.[147,148] To expedite cancer biomarker detection, which is commonly lengthy, laborious, and/or expensive, there is the need to implement a prior step of sample pretreatment to deplete HSA and IgG, ideally simultaneously concentrating lower abundant cancer biomarkers.[10]

The most used pretreatment techniques to reduce the proteomic content of HSA and IgG are liquid-liquid extraction (LLE),[11,12] solid phase extraction (SPE)[13,14] and protein precipitation (PP).[15,16] LLE is one of the most commonly used pretreatment techniques.[149] The principle of LLE involves transferring an analyte from an aqueous matrix into an extraction solvent, which should be immiscible in the aqueous matrix so that the two liquids can easily be separated.[149] Common extraction solvents include toluene, chloroform, hexane, and dichloromethane, as well as sodium chloride solutions.[150] LLE was reported as a pretreatment technique that allow the extraction of acyclovir from human serum, using dichloromethane-isopropyl alcohol as an extracting solvent.[151] The method was shown rapid, simple and reproducible with a limit of quantification of 10 ng/mL for 1 ml of serum.[151] LLE presents advantages such as high analyte recoveries and clean extracts, and is perceived as being of low cost.[149] However, it requires the consumption of large amounts of organic solvents, a large sample volume and long extraction times.[152]

The basic principles of SPE and LLE are similar, once both methods involve the distribution of dissolved samples between two phases. However, SPE requires the dispersion of the analyte between a liquid (sample medium) and a solid (adsorbent) phase,

allowing the purification and enrichment of the analytes on a solid adsorbent through adsorption from the solution.[18] The compounds retained on the solid phase can be removed by an eluting solvent, and posteriorly recovered and quantified. There is a wide choice of sorbents for SPE, including nonpolar, polar, ion exchange and mixed mode chemistries.[18] SPE has been demonstrated to be a reliable and cost-effective technique for the selective isolation and concentration of a wide range of biomolecules from sample matrices,[153] but it often exhibits limited selectivity and/or sensitivity.[18] Immunodepletion, a type of solid-phase extraction, also known as antibody-based depletion of high-abundance proteins, is a popular pretreatment technique commonly used in complex samples.[154,155] This method is based on the selective non-covalent interaction between antibodies and their specific binding to target proteins, with the purpose of removing the most abundant proteins or enriching low abundant ones.[155] Nowadays, most immunodepletion kits are chromatographic matrices (columns) or other resins with immobilized antibodies used to specifically capture target proteins/peptides. The resulting flow-through fraction (immunodepletion) or bound fraction (immunoenrichment) is collected for further analyses.[156,157] Examples of common immunodepletion kits are Seppro IgY14 kit that can deplete the 14 most abundant proteins, and Multiple Affinity Removal System columns that target the 6, 7 or 14 most abundant proteins from serum, including IgG and HSA.[158] Despite their high specificity, immunodepletion kits present some disadvantages, such as high cost and inefficiency in protein depletion resulting from the limited number of binding sites for each antibody.[158]

PP is one of the earliest proposed sample preparation technique and involves denaturation (loss of tertiary and secondary structures) of proteins present in the biomatrix.[149] The operating principle is based on the addition of an organic solvent, acid, metal, or salt to the sample under analysis.[159] For example, when an organic solvent is added to the plasma sample, it leads to a displacement of water from the hydrophobic region of the protein surface, which leads to the disruption of hydrophobic interactions between the proteins in the sample, thus causing proteins to precipitate out of solution.[159] Addition of ethanol to a serum sample has been reported to cause precipitation of IgG and most of HSA, allowing the concentration of low molecular weight proteins.[160] Some advantages of PP are the simplicity of the process, use of inexpensive reagents, and minimal loss of sample.[161] However, the process of protein precipitation presents lack of sensitivity and possible biomarker losses.[19]

To overcome performance, execution, and cost-effectiveness limitations, while avoiding biocompatibility and environmental problems displayed by common pretreatment techniques, alternative strategies are on high demand. Recently, in a review by Lee et al.,[158] authors suggested alternative materials comprising bacterial nitrocellulose, molecular imprinted polymers and cryogels as some of the most promising tools for human serum pretreatment. However, authors called the attention to the fact that most of these nanomaterials are not commercially available and their synthetic routes are complex to be implemented within most clinical and biology laboratories.[158] Alternatively, aqueous biphasic systems (ABS) can be envisaged as viable pretreatment techniques.[162,163] In addition to the possibility of integrating separation and concentration of target proteins within a single step while providing a gentle environment, ABS are of simple and fast execution and most of their components are commercially available.[20,164]

1.4.1. AQUEOUS BIPHASIC SYSTEMS (ABS) AND THREE-PHASE PARTITION (TPP)

ABS were discovered in 1896 when Beijerinck observed that a mixture containing water, gelatin and agar could generate a biphasic system.[165] However, its real application in liquid-liquid extraction for the separation of biological products was only presented in the early 1950s by Albertsson.[21] The author proposed the use of ABS formed by polyethylene glycol (PEG) and dextran (DEX) or PEG and salts, where water is the major component (instead of organic solvents as observed with typical LLE). Since then, ABS have been used for the separation, extraction, and purification of several biomolecules, including proteins, enzymes, DNA, monoclonal antibodies, and antibiotics.[166]

ABS are at least ternary systems constituted by water and a minimum of two water-soluble components, conventionally polymers[167] and salts,[168] but also short-chain alcohols,[169] surfactants,[170] and ionic liquids (ILs)[22], among others. Polypropylene glycol (PPG), polyethylene glycol (PEG), poly(ethylene glycol-ran-propylene glycol) (UCON) and DEX are examples of polymers commonly used, while citrates, phosphates, sulfates and tartrates are among the most applied salt types.[171–174] In ABS, and under specific conditions of temperature and pH, above a given concentration of the both components, two immiscible coexisting aqueous phases are formed, with a clear interfacial boundary separating the two phases, each one richer in one of the two components in addition to water.[21] The partitioning of a molecule, such as a protein, is influenced by its affinity for each phase, as well as other variables, including pH, temperature and system

composition.[175] For instance, in the conventional polymer/salt ABS, the top phase is usually enriched in the polymer, while the bottom (denser) phase is enriched in the salt.[165] Thus, it is possible to adjust the properties and affinities of the phases for any intended molecule by the suitable choice of the ABS phase-forming components, their compositions and phase separation conditions. Moreover, ABS show advantages over traditional LLE methods, like being eco- and bio-friendlier, offering mild conditions to carry out the extraction of biomolecules with no major structural, stability or activity losses.[176] If the phase-forming components are adequately selected, ABS can be created using biodegradable and biocompatible components instead of using volatile organic solvents.[165]

The characterization of ABS is performed through the determination and analysis of their phase diagrams. These are usually presented in an orthogonal representation where the mass fraction of the phase-formers is shown in the two axis and the mass fraction of water corresponds to that necessary to complete 100 wt% of the mixture composition.[177] The binodal curve (black line in Figure 6) separates the compositions that form two immiscible aqueous phases (above the binodal curve) from those that form a homogeneous single phase (below the binodal curve). The binodal curve is most often determined by the cloud-point titration method, by the visual identification of the turbid/limpid points (related data symbolized by blue circles in Figure 6).[178] The tie-lines (TLs, yellow line in Figure 6) are straight lines that connect the compositions of the top and bottom phases (points T and B in Figure 6) for a biphasic mixture. The tie-line length (TLL) indicates the distance between the two phases' compositions and decreases as the concentrations of the two water-soluble components are reduced. Mixture points located throughout the same TL have the same phases' composition but differ on the phases' volumetric/mass ratios (points A_0, A_1 and A_2 in Figure 6).[178] This feature facilitates the application of ABS within cancer diagnosis and prognosis as it enables to define the number of times a molecule of interest can be concentrated in a ABS phase (i.e., the so-called concentration factor). Finally, the point on the binodal curve where compositions of the two coexisting phases are equal is called the critical point (point C in Figure 6).

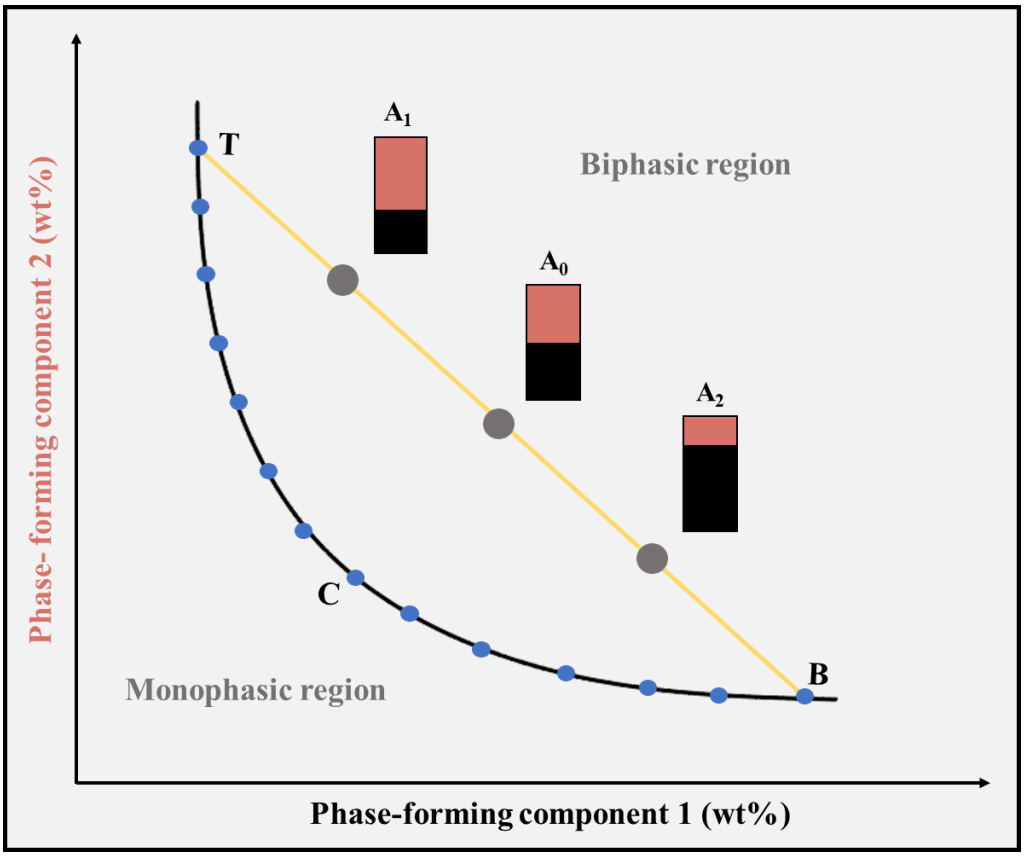

Figure 1.6. Phase diagram of an ABS in an orthogonal representation. The line T-B is the tie-line. Points A_0, A_1 e A_2 represent different compositions of the ABS and point C correspond to the critical point. (Adapted from[20])

Another useful feature of ABS in the design of novel sample pretreatment techniques is the possibility of creating three-phase partitioning (TPP) systems. Originally, TPP were firstly introduced in 1972 by Tan and Lovrein[179] and, ever since, it has been seen as a promising alternative to conventional extraction and separation methods, in particular for proteins.[180] Conventionally, TPP uses t-butanol and an aqueous solution of ammonium sulphate to promote the precipitation of target molecules, mostly proteins, at the interphase of two liquid phases. Partitioning using ABS has proved to be a valuable tool for separating and purifying mixtures of biomolecules, mainly proteins and enzymes, via extraction.[181] Although TPP is an efficient, fast and simple method, it usually requires large amounts of volatile organic solvents.[182] It has been recently shown that when certain complex matrices, such as cell culture supernatants or human serum, are added to an ABS, their components may partition between the two aqueous phases and/or precipitate at the interphase of the system. When the formation of a precipitate at

the interphase of the ABS is allowed, a TPP is generated with high water content and no need of volatile organic solvents, according to Figure 7.[26,175,183,184]

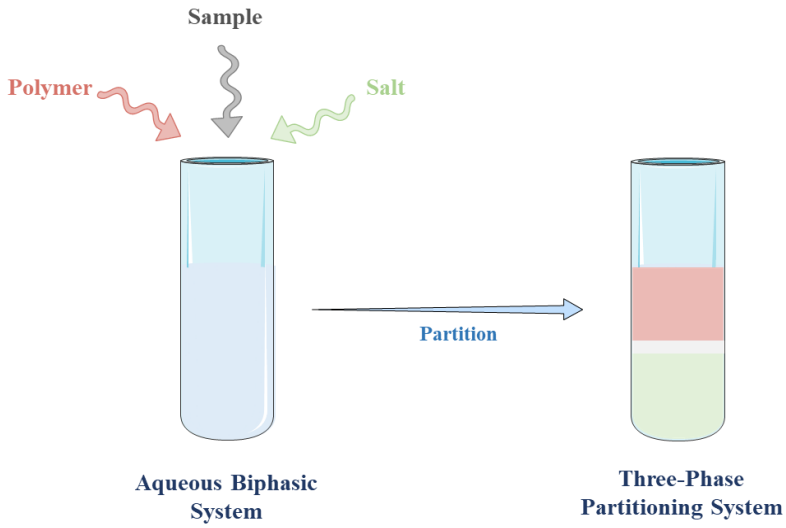

Figure 1.7. TPP formation by taking advantage of ABS concept. (Adapted from[175])

A survey of articles focused on the application of ABS or ABS-inspired TPP in the field of biomarkers' extraction and concentration is provided in Table 2. Polymer-based ABS (mostly composed of PEG/DEX) are the most studied type of systems,[23–25,185,186] notwithstanding others comprising ILs[22,26] and/or TPP-based approaches[22,26] have been reported as well. Several biomolecules found in biological fluids, mostly plasma/serum, but also urine and cell cultures, were target of attention. These include alkaline phosphatase,[185] prostate-specific antigen (PSA),[22,187] prohibitin-1[186] and extracellular vesicles (EV's),[23–25] among others,[188–190] which can be useful in the diagnosis and prognosis of oncologic, bone, immune and other disorders.[23,185,187,188,190]

Given the increasing impact of cancer in modern societies, oncologic diseases are among the most focused in ABS applications, particularly prostate and pancreatic cancers.[22,186] Regarding the application of the widely employed polymer-based ABS based on PEG/DEX, several works reported on the isolation of protein biomarkers and EVs. In the case of protein biomarkers, Zhong et al.[186] proposed the utilization of an ABS constituted by PEG/DEX (6.4 wt%/6.4 wt%) to further detect prohibitin-1, which is useful in pancreatic cancer diagnosis. The authors used a modified ABS combined

Table 1.2. Examples of application of ABS or ABS-inspired TPP in sample pretreatment and diagnosis. (ND = Not determined; NR = Not reported; NI = Not identified)

Approach	Phase-forming agents	Biomarker	Disease	Sample	Performance	Biomarker quantification technique	Ref
ABS	PEG/DEX	Alkaline phosphatase	Bone disease	Serum	ND	NR	[185]
ABS	PEG/DEX	EV'S	Prostate cancer	Urine	Recovery efficiency of 97.19%	PCR, ELISA and NTA	[24]
ABS	PEG/DEX	EV's	Prostate cancer	Plasma	Recovery efficiency of 68.3%	ELISA	[25]
ABS	PEG/DEX	EV's	Various	Plasma	Recovery efficiency of 83.4%	NTA	[23]
ABS	PEG/DEX	Prohibitin-1	Pancreatic cancer	Cell cultures	ND	Electrophoresis/ Spectrometry	[186]
ABS	PEG/DEX	TNFR1, HGF and elafin	Various	Plasma	ND	ELISA	[190]
ABS	PEG/ KH_2PO_4	Transferrin	Immune diseases	Serum	10-fold improvement in the detection limit	LFA	[188,189]
ABS	NI	PSA	Prostate cancer	Urine	Improved diagnostic performance	ND	[187,191]
ABS	$[P_{4444}][CHES]$/ $K_3C_6H_5O_7$	PSA	Prostate cancer	Urine	Recovery efficiency of ~100%	SE-HPLC	[22]
TPP	AGB-ILs/ $K_3C_6H_5O_7/C_6H_8O_7$	Transferrin	Alcoholism	Serum	Extraction efficiencies of ~100%	SE-HPLC	[26]

TPP	$[P_{4444}][(Cl/Br)]/K_3C_6H_5O_7/C_6H_8O_7$	LDH	Several cancers	Serum	Extraction efficiencies of ~100%	SE-HPLC	[26]

with two-dimensional (2D) matrix-assisted laser desorption ionization (MALDI) time of flight (TOF) mass spectrometry (MS, 2D-MALDI-TOF-TOFMS/MS) analysis to isolate and identify membrane proteins in pancreatic cancer cells. This system allowed the isolation of 55 proteins, of which 31 were membrane proteins, being associated with cell signal transduction, differentiation, and apoptosis. Prohibitin-1 was one of the mitochondria membrane proteins successfully identified using ABS, and which levels correlate with pancreatic carcinoma differentiation.[186] Several works have exploited the application of ABS in the extraction and concentration of EVs from biological fluids, their miniaturization using microfluidics and the integration of concentration and detection steps.[23] Park et al.[25] proposed the utilization of ABS formed by PEG/DEX (21 wt%/9 wt%) to isolate EVs from plasma, which play an important role in prostate cancer development and progression. The authors compared the EVs recovery efficiencies using ultracentrifugation, ExoQuick® kit, and ABS, and showed that the ABS recovered 68.3% of EVs from EV-protein mixture, whereas ultracentrifugation recovered only 15.2% and ExoQuick® recovered only 38.8%.[25] Shin et al.[24] used an optimized ABS constituted by PEG and DEX, in the same composition, to isolate EVs from a distinct biological fluid, i.e., urine. A recovery efficiency of circa 97% was obtained, which is 14 times higher than that obtained by ultracentrifugation.[24] The detection of EVs by ELISA demonstrated that the diagnosis ability when applying ABS is better than other conventional methods.[24] More recently, Han et al.[23] proposed a simple microfluidic ABS, formed by PEG and DEX (3.5 wt%/1.5 wt%), for EVs separation from small volumes of plasma. After the isolation of EVs from the plasma using the microfluidic ABS, the concentration of EVs was measured using nanoparticle tracking analysis (NTA), where a recovery efficiency of 83.4% was obtained together with a removal of 65.4% of the proteins from the EV–protein mixture.[23]

In general, a more accurate diagnosis can be obtained by the analysis of multiple biomarkers. Frampton et al.[190] studied different biomarkers, namely hepatocyte growth factor (HGF), elafine, and tumor necrosis factor receptor 1 (TNFR1), which are used in the detection of several pathologies, such as Graft-versus-host disease (GVHD). The authors reported that ELISA tests using ABS composed of PEG/DEX (20 wt%/20 wt%), provides multiplex biomarker detection for validation of new biomarker panels and diagnosis of complex diseases, where custom multiplex immunoassays are required.[190]

All works previously discussed show that PEG/DEX-based ABS are suitable for the extraction and concentration of cancer biomarkers from distinct biological samples

allowing detection. It should be however highlighted that these systems may find application in the diagnosis of other types of diseases. An example is represented by the bone diseases field, where Raymond et al.[185] showed that a PEG/DEX (30 wt%/30 wt%) system is capable of separating alkaline phosphatase, an important biomolecule in the diagnosis of bone diseases, from its isoforms. The authors reported that different partition behaviors of the alkaline phosphatase isoforms are based on the type of surfactants applied and specific anchoring interactions, which allow the selective separation.[185] Although promising recovery values were reported with PEG/DEX-based ABS (up to 97.19% with urine and up to 83.4% with serum/plasma),[23,24] these have a narrow polarity range. Therefore, polymer-based systems usually lead to low selectivity and limited pretreatment efficiency, particularly if considering serum as the biological fluid. These unmet needs can be addressed by using ILs as ABS phase-forming agents.

ILs are "designer solvents" whose structure can be finely adjusted to expand the polarity range of the ABS, thus improving extraction efficiency and selectivity.[177,192] In this line, Pereira et al.[22] developed an IL-based ABS to simultaneously extract and concentrate PSA, the gold standard for prostate cancer detection, from urine. ILs investigated were formed by the tetrabutylphosphonium ($[P_{4444}]^+$) cation and several good buffers-derived anions, including 2-(N-morpholino)ethanesulfonate ($[MES]^-$), 2-[[1,3-dihydroxy-2-(hydroxymethyl)propan-2-yl]amino]ethanesulfonate ($[TES]^-$), 2-(cyxlohexylamino)ethanesulfonate ($[CHES]^-$), 2-[4-(2-hydroxyethyl)piperazin-1-yl]ethanesulfonate ($[HEPES]^-$) and N-2(2-hydroxy-1,1-bis(hydroxymethyl)ethyl)glycine ($[Tricine]^-$). These were combined with citrate buffer ($K_3C_6H_5O/C_6H_8O_7$) as the salting-out agent. Two mixture compositions were studied: 30 wt% of IL + 30 wt% of salt and 30 wt% of IL + 40 wt% of salt. Remarkably, the authors observed a complete extraction of PSA to the IL-rich phase (extraction efficiency of 100%), in all the ABS tested for both mixture compositions, and a concentration of PSA at least up to 250-fold, with the ABS formed by $[P_{4444}][CHES]$, allowing its quantification by SE-HPLC.[22]

Several works reported ABS as a pretreatment technique associated with portable detection and quantification methods, such as the lateral-flow immunoassay (LFA).[188,189] LFA is an inexpensive point-of-care (POC) paper-based diagnostic device with the potential to rapidly detect disease biomarkers but is limited by its sensitivity.[193] Chiu et al.[188,189] used ABS containing PEG and potassium phosphate salt (KH_2PO_4), with volume ratios varying between 1:1 and 9:1 to improve the sensitivity of LFA. The authors used dextran-coated gold nanoparticles (DGNPs) anchored with specific antibodies for the

detection of transferrin, observing a preferential partition of the DGNPs for the salt-rich phase.[188,189] Then the DGNPs were used in the detection step of transferrin by LFA, and the authors reported that the previous step of concentration using ABS allowed a reliable and rapid detection of transferrin by LFA. Furthermore, through the correct choice of the volumetric ratio of the phases, it is possible to obtain improvements between 10 (9:1) and 100 (1:1) times in the detection limit of transferrin, revealing its effectiveness in improving the detection of biomarkers of interest.[188,189]

Even though promising results were so far obtained, the applicability of ABS-mediated diagnosis in clinical care remains underexplored. The works previous exposed do not study samples from real patients, or use very small donor populations, which limits their commercialization and application in a real context. The solvent interaction analysis (SIA) method proposed by Zaslavsky et al.[194] is based on analytical applications of the method of partitioning in ABS. The SIA technology is a simple and inexpensive technique that can be used for the characterization and analysis of individual proteins and their interactions with other proteins in biological samples, such as serum or plasma.[194] Thus, this method presents new opportunities for discovery and monitoring of protein biomarkers.[194] These promising characteristics are the basis for the company Cleveland Diagnostics, Inc., which is about to commercialize a technology, named IsoPSA™, that is based on the PSA partitioning between the two ABS phases and can be used for the early diagnosis of prostate cancer.[187] Several ABS were screened to develop conditions providing different partition behavior of PSA in urine samples from patients with prostate cancer and PSA from patients with benign prostate diseases.[187] The different partition coefficients of PSA obtained were sufficient for the development of the PSA/SIA test, conferring a better diagnostic performance than conventional protein biomarker detection methodologies, including tests of total serum PSA level.[191]

Another approach that can be used in the pretreatment of biological fluids, mostly human serum, combines ABS and TPP concepts to simultaneously deplete major serum proteins and concentrate the biomarker of interest. Recently, Pereira et al.[26] demonstrated that upon serum addition to an ABS, a precipitate is formed at the interphase, yielding a TPP. The systems studied were formed by glycine-betaine-based or phosphonium-based ILs and $K_3C_6H_5O_7/C_6H_8O_7$. While IgG and HSA are depleted by precipitating at the interphase of the system with depletion efficiencies of 100% in a single-step, lower abundant proteins are extracted to, and can be quantified in, the IL-rich phase.[26] This approach was successfully applied to the extraction and quantification of two biomarkers

from human serum, namely transferrin, a biomarker used for monitoring alcohol use, and LDH, a prognostic biomarker of lung and prostate cancer.[26] It should be remarked that, so far, these ABS-inspired TPP are the most efficient techniques to carry out the pretreatment of human serum prior biomarkers' detection.

Based on these previous results, the objective of the present work is to develop novel strategies for the pretreatment of human serum, taking advantage of ABS features to develop new TPP systems. To the best of our knowledge, for the first time ABS-inspired TPP composed of copolymers and salts will be investigated as human serum pretreatment techniques envisioning diagnosis/prognosis improvements. This work will focus on biomarker PTX-3 to assess the usefulness of TPP to improve the diagnosis and prognosis of lung cancer.

II – MATERIALS AND METHODS

2.1. MATERIALS

The ABS studied in this work were formulated using homopolymers/copolymers and a citrate-based salt. The homopolymers studied include polyethylene glycols (PEGs) of different molecular weights, namely 400, 600, 1000 and 2000 $g \cdot mol^{-1}$ (herein abbreviated as PEG 400, PEG 600, PEG 1000 and PEG 2000, respectively), all from Alfa Aesar, except PEG 400 and polypropylene glycol (PPG) of average molecular weight 400 $g \cdot mol^{-1}$ (PPG 400) that were acquire from Sigma-Aldrich. The homopolymers structures are depicted in Figure 2.1. The copolymers used included Pluronic PE6200 and Pluronic PE6400 (PEG-block-PPG-block-PEG-block), from BASF, Pluronic L35 (PEG-block-PPG-block-PEG-block) from Sigma-Aldrich, and UCON (PEG-ran-PPG-ran-PEG) from Sigma-Aldrich. The copolymers molecular weight (Mw), percentage of PEG (%PEG) and number of monomers of ethylene glycol ($-EG_n-$) and propylene glycol ($-PG_n-$) are represented in Table 2.1. The salt potassium citrate tribasic monohydrate ($K_3C_6H_5O_7 \cdot H_2O$, purity ≥ 99%) was obtained from Acros Organics and citric acid ($C_6H_8O_7.H_2O$, purity ≥ 99.5%) from Panreac.

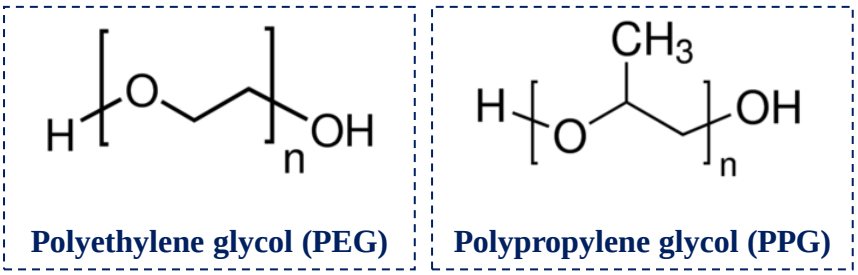

Figure 2.1. Chemical structure of the homopolymers used in this work.

Table 2.1. Molecular weight (Mw), percentage of PEG monomer (%PEG), number of ethylene glycol monomers ($-EG_n-$) and number of polypropylene glycol monomers ($-PG_n-$) of the phase forming copolymers studied.

Copolymers	Mw ($g \cdot mol^{-1}$)	%PEG	($-EG_n-$)	($-PG_n-$)
Pluronic PE6200	1750	20	11	28
Pluronic PE6400	1750	40	13	20
Pluronic L35	1900	50	11	16
UCON	2500	50	-	-

The human serum used was obtained from Sigma-Aldrich (H4522- Lot # SLBX6353) and kept at -20ºC up to use. For the preparation of the IgG solution, a solution of human IgG purified (29.4 mg/mL) was used, purchased from Innovative Research, Inc. and kept in storage at -80 ºC. The solution of HSA was prepared using a lyophilized powder of albumin from human (purity ≥ 96%) obtained from Alfa Aesar. Pentraxin-3 (purity ≥ 90%) was obtained from Sigma-Aldrich Chemical Co. The quantification of PTX-3 was performed using a commercially available enzyme-linked immunosorbent assay (ELISA) kit (ab214570), purchased from abcam and kept in storage at 4ºC.

2.2. DETERMINATION OF PHASE DIAGRAMS AND TIE-LINES

To establish the mixture compositions required to form systems with two coexisting phases that can be used as extraction tools, ternary phase diagrams for the homopolymers PPG 400, PEG 400, PEG 600, PEG 1000 and PEG 2000, and for the copolymers Pluronic PE6200, Pluronic PE6400, Pluronic L35 and UCON were determined at pH ≈ 7. The buffer $K_3C_6H_5O_7/C_6H_8O_7$ at 50 wt% was used to maintain the pH of the overall ABS at the desired value. The binodal curve of each ABS was determined through the cloud point titration method[177] at 25 (± 1) ◦C and atmospheric pressure. Aqueous solutions of salt at circa 50 wt% and aqueous solutions of the different polymers/copolymers (with concentrations ranging from 30 wt% to 70 wt%) were prepared and used for the determination of the phase diagrams. Repeatedly and under continuous stirring, drop-wise addition of the aqueous buffered solution to the homopolymer/copolymer solution was done until getting a cloudy solution (biphasic region), followed by the drop wise addition of water until a clear and limpid solution is encountered (monophasic region), as Figure 2.2 outlines. The ternary system compositions after the addition of each component were determined by weight quantification within an uncertainty of ± 10^{-4} g.

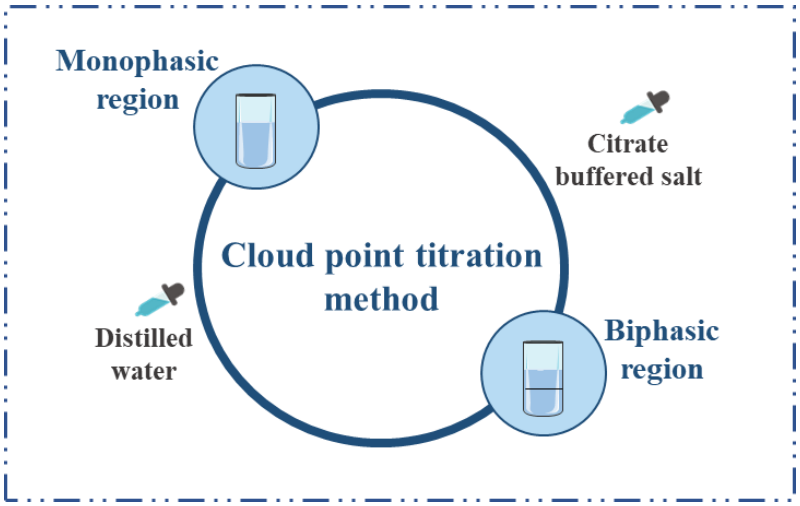

Figure 2.2. Schematic representation of the cloud point titration method.

The tie-lines (TLs) of each phase diagram were determined by a gravimetric method described by Merchuk et al.[195], using mixture compositions where all systems are within the two-phase region. The selected mixtures were prepared by weighting the proper quantity of homopolymer/copolymer + $K_3C_6H_5O_7/C_6H_8O_7$ buffer + water. Then, each mixture was vigorously stirred, centrifuged for 10 min at 3500 rpm and left in equilibrium for more 10 min at 25°C to ensure equilibration of the coexisting phases. After separation of the two phases, each phase was carefully weighted within an uncertainty of ± 10^{-4} g. Each individual TL was determined by the application of the lever-arm rule to the relationship between the weight of the top and bottom phases and the overall system composition. To ascertain with accuracy the monophasic/biphasic regions, the experimental points obtained to determine the binodal curve were correlated using the three-parameter equation, proposed by Merchuk and collaborators[195]:

$$[Y] = Aexp\,(B[X]^{0.5} - C[X]^3) \qquad (2.2.1)$$

where [Y] and [X] represent the weight fractions (wt%) of polymer/copolymer and salt, respectively, and A, B, and C correspond to the adjusted parameters obtained by least-squares regression. For the determination of the TLs the following system of four equation (Equations 2.2.2 to 2.2.5) was used to calculate the concentration of polymer/copolymer and salt at each phase ($[Polymer]_{Top}$, $[Salt]_{Top}$, $[Polymer]_{Bot}$ and $[Salt]_{Bot}$):

$$[Polymer]_{Top} = Aexp\ [(B[Salt]_{Top}^{0.5}) - (C[Salt]_{Top}^{3})] \quad (2.2.2)$$

$$[Polymer]_{Bot} = Aexp\ [(B[Salt]_{Bot}^{0.5}) - (C[Salt]_{Bot}^{3})] \quad (2.2.3)$$

$$[Polymer]_{Top} = \frac{[Polymer]_M}{\alpha} - \left(\frac{1-\alpha}{\alpha}\right)[Polymer]_{Bot} \quad (2.2.4)$$

$$[Salt]_{Top} = \frac{[Salt]_M}{\alpha} - \left(\frac{1-\alpha}{\alpha}\right)[Salt]_{Bot} \quad (2.2.5)$$

where the subscripts "Top", "Bot" and "M" represent the top phase, the bottom phase, and the mixture composition, respectively. The parameter α is the ratio between the top phase and the total weight of the mixture. For the calculation of each tie-line length (TLL) the equation 6 was applied.

$$\text{TLL} = \sqrt{([Salt]_{Top} - [Salt]_{Bot})^2 + ([Polymer]_{Top} - [Polymer]_{Bot})^2} \quad (2.2.6)$$

2.3. pH MEASUREMENT

The pH values of both the top phase (polymer-rich phase) and the bottom phase (salt-rich phase) were measured at 25 ºC using a pH/Conductometer from Metrohm within an uncertainty of ± 0.02. To calibrate the pH meter two buffers, also from Metrohm, with pH values of 4.00 and 7.00 were used.

2.4. DEPLETION OF HSA AND IgG IN HUMAN SERUM

After gathering the knowledge on the mixture compositions needed to form aqueous biphasic systems by the determination of the phase diagrams, a mixture point where all systems are within the two-phase region was selected to study the partition behavior and/or depletion of HSA and IgG. The mixture composition used was: 30 wt% of homopolymer/copolymer, 30 wt% of $K_3C_6H_5O_7/C_6H_8O_7$ buffer, 5% of human serum and 35% of water. Two replicas were prepared for each system. ABS were prepared by weighting the appropriate amount of each component, within ± 10^{-4} g, and mixing until all components were dissolved. Each mixture was stirred, centrifuged for 10 min at 3500 rpm, and left to equilibrate for 10 min at 25ºC to reach total phase separation and to ensure HSA and IgG depletion, that should ideally precipitate at the interphase. After the equilibrium conditions, both phases were carefully separated, and the precipitate was diluted in a phosphate buffer solution (PBS). The amount of HSA and IgG in each phase

was quantified by SE-HPLC. The equipment used was a Chromaster HPLC system (VWR Hitachi) equipped with an analytical column (8 mm × 300 mm), Protein KW-802.5, from Shodex, with a 50 mM sodium phosphate buffer + NaCl 0.3 M, run isocratically with a flow rate of 0.5 $mL.min^{-1}$. The column oven and autosampler temperatures were kept at 25°C and at 10°C, respectively. The injection volume was of 25 µL and the wavelength was set at 280 nm, whereas the retention time of IgG and HSA was 15.21 and 16.60 min, respectively. The quantification of these proteins in each phase was carried out using calibration curves previously established for IgG (R^2 = 0.9989) and HSA (R^2 = 0.9989), depicted in Appendix.

The ABS performance to deplete IgG and HSA from commercial human serum by inducing their precipitation at the interphase was evaluated by their depletion efficiencies (DE_{IgG}% and DE_{HSA}%), according to the following equations:

$$DE_{IgG}\% = \frac{w_{IgG}^{Int}}{w_{IgG}^{Top} + w_{IgG}^{Int} + w_{IgG}^{Bot}} \times 100 \quad (2.4.1)$$

$$DE_{HSA}\% = \frac{w_{HSA}^{Int}}{w_{HSA}^{Top} + w_{HSA}^{Int} + w_{HSA}^{Bot}} \times 100 \quad (2.4.2)$$

where w_{IgG}^{Top}, w_{IgG}^{Int} and w_{IgG}^{Bot} represent, respectively, the weight of IgG in the top phase, in the interphase and in the bottom phase, and w_{HSA}^{Top}, w_{HSA}^{Int}, w_{HSA}^{Bot} represent the weight of HSA in the top phase, in the interphase and in the bottom phase, respectively.

2.5. EFFECT OF SAMPLE COMPLEXITY ON DEPLETION EFFICIENCIES

The relevance of sample complexity on IgG and HSA precipitation at the interphase was analyzed. To this end, the ABS performance to deplete these proteins was evaluated using three solutions with different protein compositions, represented in Table 2.2. The mixture point with a composition of 30 wt% of homopolymer/copolymer and 30% of $K_3C_6H_5O_7/C_6H_8O_7$ buffer was used and 0.1 g of each diluted solution (1:2) was directly applied in each aqueous solution. Two replicas were prepared for each system.

Table 2.2. Solutions used to study the influence of different protein compositions on the protein distribution among the three phases.

Solution	[HSA] / (mg/mL)	[IgG] / (mg.mL^{-1})
HSA	42	0
IgG	0	12
HSA + IgG	42	12

Each ABS was prepared by weighting the appropriate amount of each component, within an uncertainty of ± 10^{-4} g. Each mixture was stirred, centrifuged for 10 min at 3500 rpm, and left to equilibrate for further 10 min at 25ºC to promote phase separation. After, a careful separation of the phases was performed and the HSA and IgG content in each phase was determined by SE-HPLC. The quantification of these proteins in each phase was carried out using calibration curves previously established for IgG and HSA, depicted in Figures A1 and A2, respectively, in the Appendix.

The ABS performance to deplete IgG and HSA from commercial human serum by inducing their precipitation at the interphase was evaluated by their depletion efficiencies (DE_{IgG}% and DE_{HSA}%), according to the equations 2.4.1 and 2.4.2, previously described.

2.6. EXTRACTION OF PTX-3 USING TPP

To evaluate the TPP ability to simultaneous deplete HSA and IgG and extract PTX-3, the systems presenting higher depletion efficiencies for both proteins were selected, corresponding to the ones formulated using PEG 1000, PEG 2000, PPG 400 and UCON. Aqueous solutions containing human serum, human serum spiked with PTX-3 (5 ng.mL^{-1}) and an aqueous solution containing only PTX-3 (5 ng.mL^{-1}) were prepared. A mixture composition of 30 wt% of the homopolymers/copolymers, 30% of $K_3C_6H_5O_7/C_6H_8O_7$ buffer and 10 wt% of each diluted aqueous solution (1:2) was used. Each system was prepared by weighting the appropriate amount of each component, within an uncertainty of ± 10^{-4} g, vigorously stirred, centrifuged for 10 min, and left to equilibrate for at least 10 min at 25ºC to reach the HSA and IgG complete depletion and the PTX-3 complete partition. After the equilibrium conditions, both phases were carefully separated, and the precipitate was diluted PBS. The concentration of PTX-3 in each phase was detected using an ELISA kit following the manufacturer's instructions

and using a calibration curve previously established, depicted in Figure A4, in the Appendix. The interference of the citrate buffered salt, polymers and proteins present in human serum samples with the quantification method were also determined and blank control samples were used. At least three independent ABS were prepared for each homopolymer/copolymer analyzed.

The percentage extraction efficiency of PTX-3 ($EE_{PTX\text{-}3}\%$) by each TPP in the polymer-rich phase is defined according to the following equation:

$$EE_{PTX-3}\% = \frac{w_{PTX-3}^{Polymer}}{w_{PTX-3}^{Polymer} + w_{PTX-3}^{Salt}} \times 100 \qquad (2.6.1)$$

where $w_{PTX-3}^{Polymer}$ and w_{PTX-3}^{Salt} are the total weight of PTX-3 in the polymer-rich phase and in the salt-rich phase, respectively.

The recovery yield of PTX-3 in the top phase, as a precipitate in the interphase and in the bottom phase ($RY_{Protein/Top}\%$, $RY_{Protein/Interphase}\%$, $RY_{Protein/Bottom}\%$) is the percentage ration between total weight of PTX-3 in the top/interphase/bottom phases to that in the initial mixture, and is defined according to equation 2.6.2:

$$RY_{PTX-3}\% = \frac{w_{PTX-3}^{Top/Interphase/Bottom}}{w_{PTX-3}^{Initial}} \times 100 \qquad (2.6.2)$$

where $w_{PTX-3}^{Top/Interphase/Bottom}$ is the total weight of PTX-3 in the top/interphase/bottom phases and $w_{PTX-3}^{Initial}$ is the total weight of PTX-3 present in the initial solution.

III – RESULTS AND DISCUSSION

3.1. PHASE DIAGRAMS AND TIE-LINES

Phase diagrams of each ternary system formed by the homopolymers PPG 400, PEG 400, PEG 600, PEG 1000 and PEG 2000, and the copolymers Pluronic PE6200, Pluronic PE6400, Pluronic L35 and UCON, with $K_3C_6H_5O_7/C_6H_8O$ buffer (pH 7.0) and water were determined at 25°C and atmospheric pressure. The binodal curves of ABS formed by homopolymers and copolymers were determined by the cloud point titration method[177] and are depicted in Figures 3.1 and 3.2, respectively. To eliminate the effects induced by the different molecular weight of polymers the binodal curves are compared in molality units in addition to those in weight fraction. The experimental weight fraction data for all the studied systems are reported in Tables A1, A2 and A3, in the Appendix.

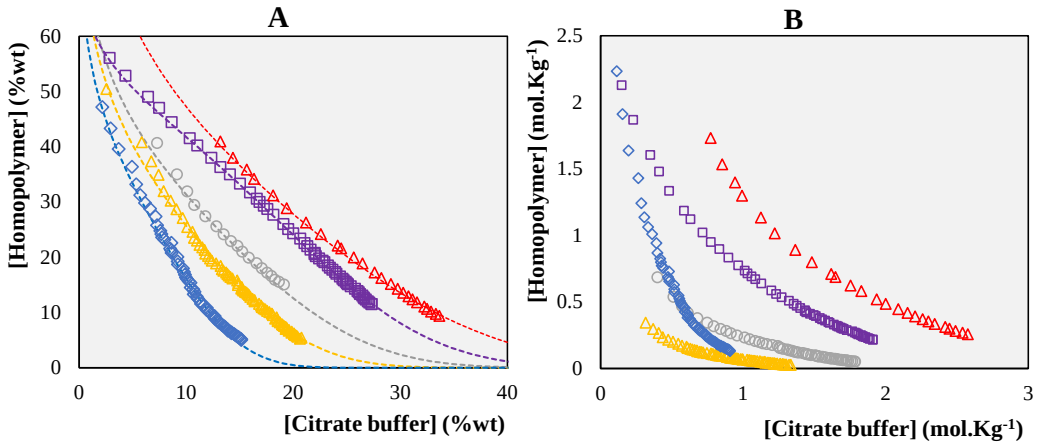

Figure 3.1. Phase diagrams for the ternary systems composed of homopolymers, $K_3C_6H_5O_7/C_6H_8O$ and water at 25°C and atmospheric pressure in weight fraction (A) and in molality unit (B): (◇) PPG 400, (△) PEG 2000, (○) PEG 1000, (◇) PEG 600, and (△) PEG 400.

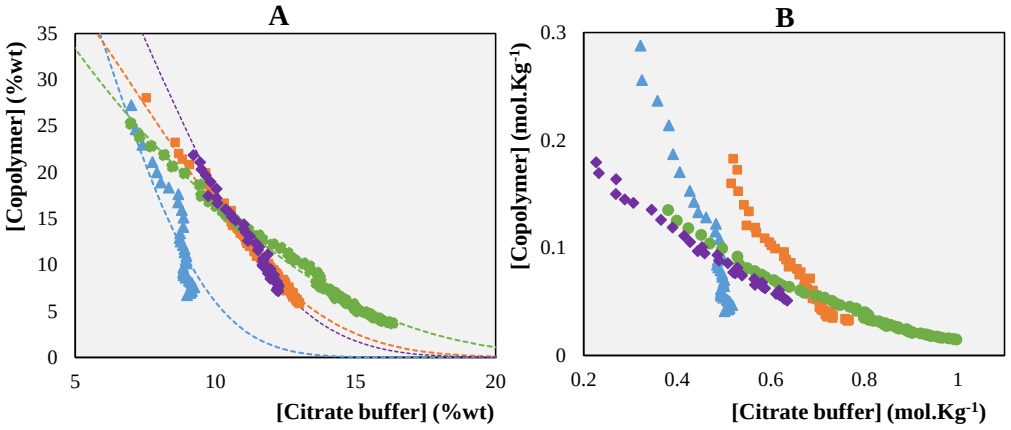

Figure 3.2. Phase diagrams for the ternary systems composed of copolymers, $K_3C_6H_5O_7/C_6H_8O$ and water at 25 ◦C and atmospheric pressure in weight fraction (A) and in molality (B): (▲) Pluronic PE6200, (■) Pluronic PE6400, (◆) Pluronic L35, and (●) UCON.

The determination of the binodal curve is crucial to design their intended application, since it gives insight on the percentage mass concentration of homopolymer/copolymer and salt needed to establish two-phase systems. Compositions of homopolymer/copolymer and $K_3C_6H_5O_7/C_6H_8O$ buffer above each binodal curve result in biphasic systems, whereas mixture compositions below the same curve fit within the monophasic regime. In systems with a larger biphasic region, the ability of both components to cause phase separation is higher, thus requiring lower amounts of polymer and citrate buffered salt to create an ABS. The citrate-based salt used in the ABS formulation is a strong salting-out species according to the Hofmeister series.[196] Since this salt is composed of a triply charged anion strongly hydrated it presents a higher affinity for water,[197] being highly effective in the exclusion of the homopolymer/copolymer from the aqueous solution, promoting the two-phase separation. In all studied ABS the bottom phase corresponds to the salt-rich phase, while the top phase is mainly composed of homopolymer/copolymer and water.

Since the salt, temperature, pressure, and pH are constant, the ABS formation ability is both dependent on the type and molecular weight of the homopolymer/copolymer. As depicted in Figure 3.1, the ability of homopolymers to create ABS, at 0.5 $mol.Kg^{-1}$ of $K_3C_6H_5O_7/C_6H_8O$ buffer, can be ranked as follows: PEG 2000 > PPG 400 > PEG 1000 > PEG 600 > PEG 400. By their turn, the copolymers' tendency of two-phase formation, at 0.15 $mol.Kg^{-1}$ of $K_3C_6H_5O_7/C_6H_8O$ buffer, according to Figure 3.2, follows the order: Pluronic L35 ≈ UCON > Pluronic PE6200 > Pluronic PE6400.

In what concerns the ability of homopolymers to induce liquid-liquid demixing, PPG is more hydrophobic than PEG due to the presence of an additional methyl group at the monomeric unit. The larger biphasic region observed with PPG 400 than with PEG 400 can thus be credited to such a structural feature. The ability of PEGs to form ABS increases with the molecular weight, i.e., PEG 2000 presents a larger two-phase region, followed by PEG 1000, PEG 600 and PEG 400. This result is related to the hydrophobicity or the lower affinity for water of polymers bearing higher molecular weights, making them easier to be excluded to the top phase by a salting-out species ($K_3C_6H_5O_7/C_6H_8O$ buffer). PEG 400 presents the lower capacity to induce two-phase separation, since this low molecular weight polymer has a higher affinity for water, requiring more citrate-buffered salt to induce the separation of the phases.

Among the copolymers, which binodal curves are represented in Figure 3.2, Pluronic PE6200 produces a larger biphasic region than Pluronic PE6400, likely due to its lower PEG percentage and thus, more hydrophobic nature. On the other hand, and although differences in the monomers' organization, the binodal curves obtained for Pluronic L35 and UCON present a similar behavior once the effect of molecular weight was eliminated.

For the sake of comparison of the ability of the studied copolymers to form biphasic systems with the corresponding homopolymers, the phase diagrams obtained for the copolymers, PPG 400 and PEG 2000 were represented in the same graph, being given in Figure 3.3.

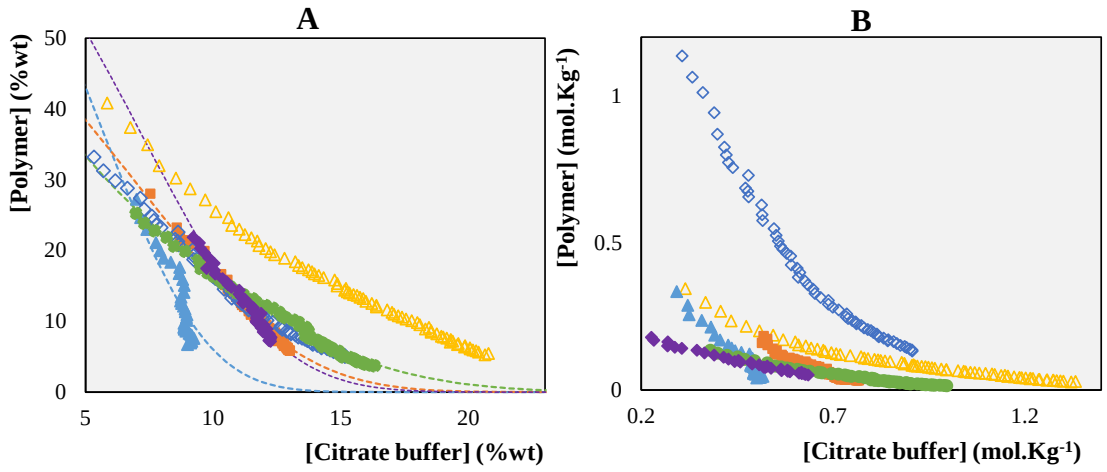

Figure 3.3. Phase diagrams for the ternary systems composed of homopolymers/copolymers, $K_3C_6H_5O_7$/C_6H_8O and water at 25 ◦C and atmospheric pressure in weight fraction (A) and in molality (B): (▲) Pluronic PE6200, (■) Pluronic PE6400, (◆) Pluronic L35, (●) UCON, (◇) PPG 400, and (△) PEG 2000.

The use of copolymers in ABS may provide either intermediary or even totally distinct properties to those of the corresponding homopolymers, thus allowing to better tune the extraction performance and selectivity of ABS. In addition, the use of copolymers allows to expand the properties usually afforded by common homopolymers, such as PEG and PPG in ABS, as disclosed by the relative position and shapes of the binodal curves. The ability of the copolymers to form ABS outpaced that of the homopolymers. Taking as reference PEG 2000 and Pluronics (that have similar molecular weights), the PPG content in the copolymers supports this behavior. Although PPG is exclusively composed of more hydrophobic monomeric units, it has a lower molecular weight and its ability to form ABS is surpassed by that of the copolymers. Finally, the amount of phase-forming

agents needed to acquire an ABS can be significantly decreased with copolymers, being also useful from an economic perspective.

Overall, the results here obtained indicate that the ability of polymers to form ABS correlates well with their hydrophobic nature, with the systems formed by the most hydrophobic ones presenting larger biphasic areas. The portfolio of ABS may be expanded by introducing homopolymers/copolymers, thus opening doors for future applications in the domain of biomolecules' extraction.

For the studied systems, the experimental data corresponding to the binodal curves were fitted using Equation (2.2.1). The regression parameters (A, B and C) were estimated by least-squares regression, and their values, as well as the corresponding standard deviations (σ) and correlation coefficients (R^2) are provided in Table 3.1.

Table 3.1. Correlation parameters used to describe the experimental binodal data obtained by equation (1) for the systems composed of homopolymer/copolymer + $K_3C_6H_5O_7$/C_6H_8O + H_2O, and respective standard deviations (σ) and correlation coefficients.

Homopolymer/ Copolymer	A ± σ	B ± σ	10^5 (C ± σ)	R^2
PPG 400	82.5198 ± 5.2691	-0.3813 ± 0.0328	0.0004 ± 4.1894	0.9766
PEG 400	118.3362 ± 16.5869	-0.2830 ± 0.0382	0.0002 ± 0.0000	0.9960
PEG 600	102.4846 ± 10.4248	-0.2806 ± 0.0306	0.0004 ± 0.0000	0.9908
PEG 1000	91.6785 ± 7.5399	-0.3168 ± 0.0286	0.0001 ± 6.0346	0.9872
PEG 2000	91.1772 ± 4.3738	-0.3572 ± 0.0190	0.0001 ± 8.135	0.9914
Pluronic PE6200	99.8726 ± 4.8299	-0.26670 ± 0.0503	0.0020 ± 0.0003	0.9775
Pluronic PE6400	77.7133 ± 7.0624	-0.2766 ± 0.0427	0.0007 ± 4.1199	0.9891
Pluronic L35	99.9889 ± 1.6878	-0.2507 ± 0.0221	0.0009 ± 0.0005	0.9955
UCON	99.9151 ± 1.0648	-0.4737 ± 0.0084	0.0004 ± 0.0000	0.9983

Overall, satisfactory correlation coefficients were obtained, and the corresponding parameters are important to predict data in a certain region of the ternary phase diagram where no experimental data are available. It is important to state that other equations can

be used to fit the binodal curve.[177] However, the equation proposed by Merchuk is frequently applied because it makes use of a lower number of adjustable parameters to correlate the data when compared with other alternative equations.[177] Furthermore, the Merchuk equation is the only one that permits the direct determination of the TLs through a mathematical approach (lever-arm rule),[195] allowing to estimate the concentrations of each ABS-forming component in the top and bottom phases and the overall system compositions.

The experimental TLs determined for each system and their respective length, as well as the weight fraction compositions for the coexisting phases are reported in Table 3.2. Since the TLL represents the difference between the homopolymer/copolymer and salt concentrations in the top and bottom phases, respectively, longer tie-lines indicate a more complete homopolymer/copolymer and salt partitioning resulting in a higher concentration of homopolymer/copolymer in the top phase and of citrate buffered salt in the bottom phase. The results reported in Table 3.2 show that TLs are longer in the ABS formed by PPG 400 and UCON and shorter in the systems composed of Pluronic PE6200 and Pluronic PE6400, indicating that the separation of the ABS-forming components is not so efficient in these two last systems. This information is relevant because the present work aims to apply these ABS in the extraction of lung cancer biomarkers, and it was shown that the top and bottom phase compositions may have an important influence in the migration of biomolecules.[198,199] The establishment of the phase diagrams and tie-lines allowed selecting the percentage of homopolymer/copolymer and salt in ABS for the depletion of HSA and IgG.

Table 3.2. Experimental TLs and TLLs obtained for the ABS composed of homopolymer/copolymer + $K_3C_6H_5O_7/C_6H_8O$ buffer + H_2O at 25°C and atmospheric pressure. (Top = Top phase; M=Mixture point; Bot= Bottom phase.)

		Weight fraction composition / (wt%)						
		$[Polymer]_{Top}$	$[Salt]_{Top}$	$[Polymer]_{M}$	$[Salt]_{M}$	$[Polymer]_{Bot}$	$[Salt]_{Bot}$	TLL
PPG 400	TL 1	93.4306	0.0000	29.8249	28.9954	0.0000	42.7956	102.8909
	TL2	95.5886	0.0000	30.2920	28.9563	0.0000	42.8564	103.9471
PEG 400	TL 1	55.2601	7.0855	30.1592	29.0319	0.3225	55.1188	72.9749
	TL 2	56.8854	6.5799	30.6396	28.7955	0.3778	54.4104	74.0328
PEG 600	TL 1	63.1040	2.9738	31.1076	28.8696	0.0255	54.0254	81.1489
	TL 2	59.8567	3.6467	30.8241	28.6551	0.0165	55.1924	78.9798
PEG 1000	TL 1	72.0947	0.5752	29.7075	29.2900	0.0019	49.4137	87.0780
	TL2	72.9693	0.5190	29.2149	29.2149	0.0022	49.1419	87.6835
PEG 2000	TL 1	71.8371	0.4454	29.0438	29.1177	0.0000	48.5775	86.4712
	TL2	72.9701	0.3889	29.2456	29.2589	0.0000	48.5688	87.4411
UCON	TL 1	76.8981	0.0000	29.3755	28.8531	0.0000	47.2063	90.5421
	TL2	77.9344	0.0000	30.0849	28.9661	0.0000	47.6843	91.6571
Pluronic PE6200	TL 1	51.3109	3.8807	31.1918	28.6981	12.4944	45.0501	56.5830
	TL2	50.3137	3.8738	31.2424	28.9386	9.7140	47.7333	59.7661

Pluronic PE6400	TL 1	67.4945	0.2597	29.9667	28.6621	0.0000	51.3420	84.6458
	TL2	73.4474	0.0417	29.9257	29.2632	0.0000	49.3561	88.4671
Pluronic L35	TL 1	72.0633	0.0000	29.7989	29.1889	0.0000	50.4294	88.2716
	TL 2	70.1414	0.0000	29.8301	29.4259	0.0000	49.7012	89.6937
UCON	TL 1	76.8981	0.0000	29.3755	28.8531	0.0000	47.2063	90.5421
	TL2	77.9344	0.0000	30.0849	28.9661	0.0000	47.6843	91.6571

3.2. DEPLETION OF HSA AND IgG IN HUMAN SERUM

After determining the composition of each component required to form two-phase systems, all the ABS herein studied were evaluated in terms of their performance as a pretreatment strategy of human serum to deplete the most abundant proteins (HSA and IgG) in a single step. The mixture composition selected was: 30 wt% of homopolymer/copolymer and 30% of $K_3C_6H_5O_7/C_6H_8O_7$ buffer. The SEC-HPLC retention time of IgG and HSA was found to be ≈ 15.21 and ≈ 16.60 min, respectively, and the chromatogram obtained for the human serum sample in aqueous solution is depicted in Figure A3 in the Appendix. The average depletion efficiencies (DE_{IgG}% and DE_{HSA}%) for the systems formed by homopolymers and copolymers are represented in Figures 3.4 and 3.5, respectively. In all systems, the top phase is homopolymer/copolymer-rich, and the bottom phase is mainly constituted by water and citrate buffered salt.

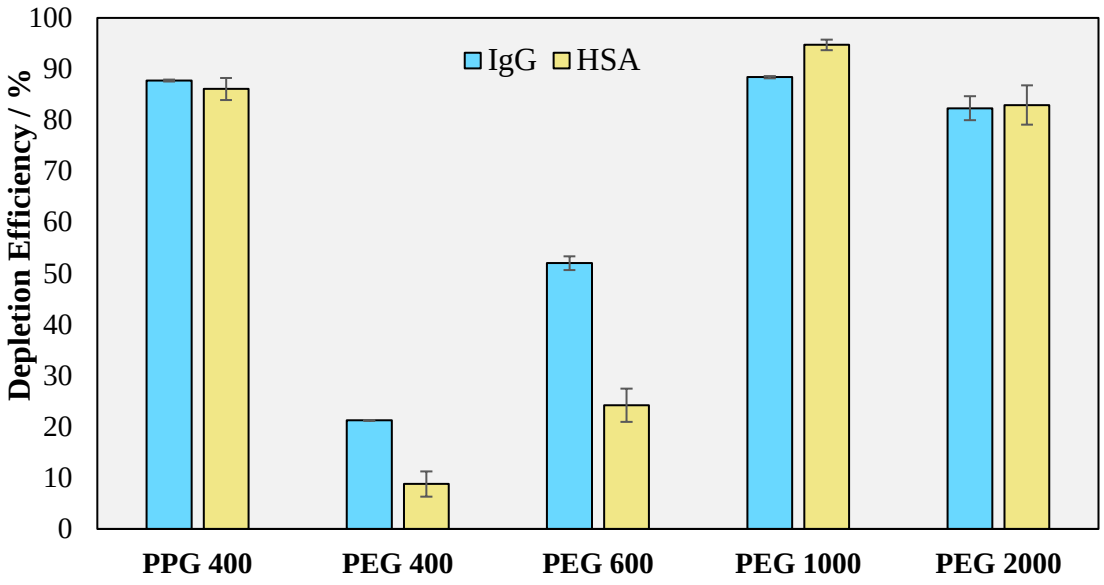

Figure 3.4. Depletion efficiencies obtained for IgG (■) and HSA (■) in ABS/TPP formulated using 30 wt% of homopolymer and 30 wt% of $K_3C_6H_5O_7/C_6H_8O_7$ buffer (pH = 7), at 25ºC and atmospheric pressure.

In the ABS/TPP composed of homopolymers depletion efficiencies ranging between 21 and 88% for IgG and between 9 and 95% for HSA were obtained. In all systems, SE-HPLC chromatograms were used for HSA and IgG quantification. Taking into account the data depicted in Figure 3.4, the TPP formed by the homopolymer PEG 1000 was the system with higher depletion efficiencies for both HSA and IgG, followed

by the systems formed by PPG 400 and PEG 2000, with the majority of HSA and IgG content precipitating at the interphase. In all these systems, the remaining proteins migrated preferentially to the top phase. In fact, in the SE-HPLC chromatograms of most systems, no IgG and HSA at the bottom (salt-rich) phase was identified.

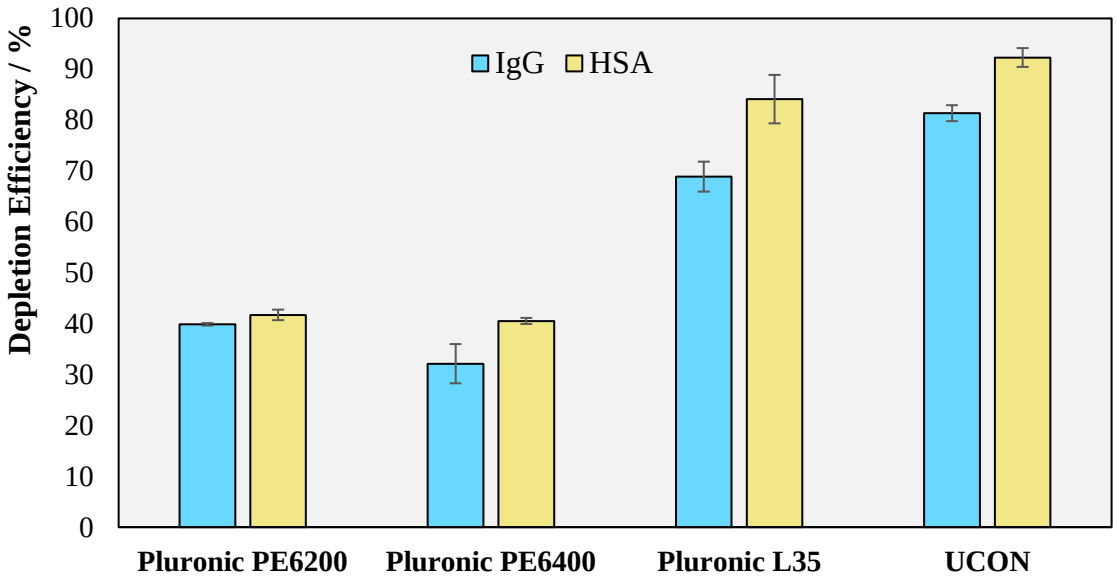

Figure 3.5. Depletion efficiencies obtained for IgG (■) and HSA (■) in TPP formulated using 30 wt% of copolymer and 30 wt% of $K_3C_6H_5O_7/C_6H_8O_7$ buffer (pH = 7), at 25ºC and atmospheric pressure.

In what concerns the TPP formulated using copolymers, single-step depletion efficiencies ranging from 32 to 81% for IgG and between 41 to 92% for HSA were achieved. The TPP formed by UCON presented higher depletion efficiencies for both HSA and IgG, followed by Pluronic L35, Pluronic PE6200 and finally Pluronic PE6400, as shown in Figure 3.5. In the systems formed by Pluronic PE6200 and Pluronic PE6400 the partitioning of HSA and IgG was mainly accomplished to the top phase, with some of the proteins precipitating in the interphase. Since the aim was to promote the precipitation of these proteins in the interphase, the significant partitioning to the top phase made these two last systems unsuitable for the target purpose.

The partitioning and solubilization of proteins in TPP is guided by several interactions established between the exposed groups of proteins and the phase-forming components. The precipitation of HSA and IgG at the interphase seems to be mainly driven by the high concentrations of polymers, which reduce the solubility of these proteins in the polymer-rich phase (top phase), together with salting-out effects. However,

hydrogen-bonding interactions cannot be discarded because of the water-rich media, as well as electrostatic interactions since extractions were carried out at pH values different from HSA isoelectric point (pI = 4.7).[177] All systems studied in this work were done under controlled pH (pH ≈ 7.0). However, after the two-phases separation, the pH values of both top and bottom phases were measured, being displayed in Table 3.3. Small deviations exist, which may be resultant from the added polymer.

Table 3.3. pH values obtained for the top and bottom phases of ABS formed by 30 wt% of homopolymer/copolymer and 30 wt% of $K_3C_6H_5O_7$/$C_6H_8O_7$ buffer, at 25 ºC and atmospheric pressure.

Homopolymer/Copolymer	pH value	
	Top phase	Bottom phase
PPG 400	7.73 ± 0.06	6.73 ± 0.01
PEG 400	7.25 ± 0.09	7.18 ± 0.04
PEG 600	7.22 ± 0.09	7.08 ± 0.00
PEG 1000	7.69 ± 0.08	7.06 ± 0.07
PEG 2000	7.18 ± 0.05	6.91 ± 0.15
Pluronic PE6200	6.51 ± 0.02	6.78 ± 0.08
Pluronic PE6400	6.53 ± 0.01	6.92 ± 0.05
Pluronic L35	7.62 ± 0.05	6.76 ± 0.03
UCON	8.48 ± 0.06	6.98 ± 0.09

The control of the pH value of the aqueous phases formed is very important since the present work aims to separate/extract proteins, whose structures are highly dependent on this variable.[200,201] The isoelectric points of HSA and IgG are 4.7 and 6.5-9.5, respectively.[202,203] Thus, in all the situations HSA is negatively charged (pH > pI) and IgG is electrically neutral (pH = pI). Proteins tend to precipitate most readily at their isoelectric point, because of the reduced repulsive electrostatic forces that cause aggregation and precipitation.[180] On the other hand, negatively charged proteins are more soluble and not easily precipitated. Even negatively charged, almost all the HSA content

precipitated at the interphase in the systems formed by PPG 400, PEG 1000, PEG 2000 and UCON, indicating that the electrostatic interactions were not relevant in the partition of this protein in these systems. In the systems composed of Pluronic PE6200 and Pluronic PE6400, and although some of HSA and IgG content precipitated at the interphase, most of these proteins migrated to the top phase. However, this occurrence does not seem to be guided by electrostatic interactions since IgG is neutral and migrated preferentially to the top phase instead of precipitating.

In conclusion, the TPP formed by the homopolymers PEG 1000, PEG 2000 and PPG 400, and the copolymers UCON and Pluronic L35 were selected as the most efficient systems for the removal of HSA and IgG content from human serum, representing a promising approach for the pretreatment of human serum samples in a single step.

3.3. EFFECT OF SAMPLE COMPLEXITY ON DEPLETION EFFICIENCIES

Human serum is an exceptionally complex fluid comprising thousands of proteins, with HSA and IgG accounting for 80% of this proteomic content.[9,204] To study the role of sample complexity in the partition of HSA and IgG in TPP, solutions containing human serum, HSA and IgG, only HSA and only IgG were analyzed. The average efficiency of each TPP formed by homopolymers/copolymers to deplete HSA and IgG from these four solutions with different protein compositions were determined and are represented in Figures 3.5 and 3.6, respectively. The detailed depletion efficiencies obtained for each ABS/TPP composed of homopolymers and copolymers are displayed in Tables A4 and A5, respectively, in the Appendix.

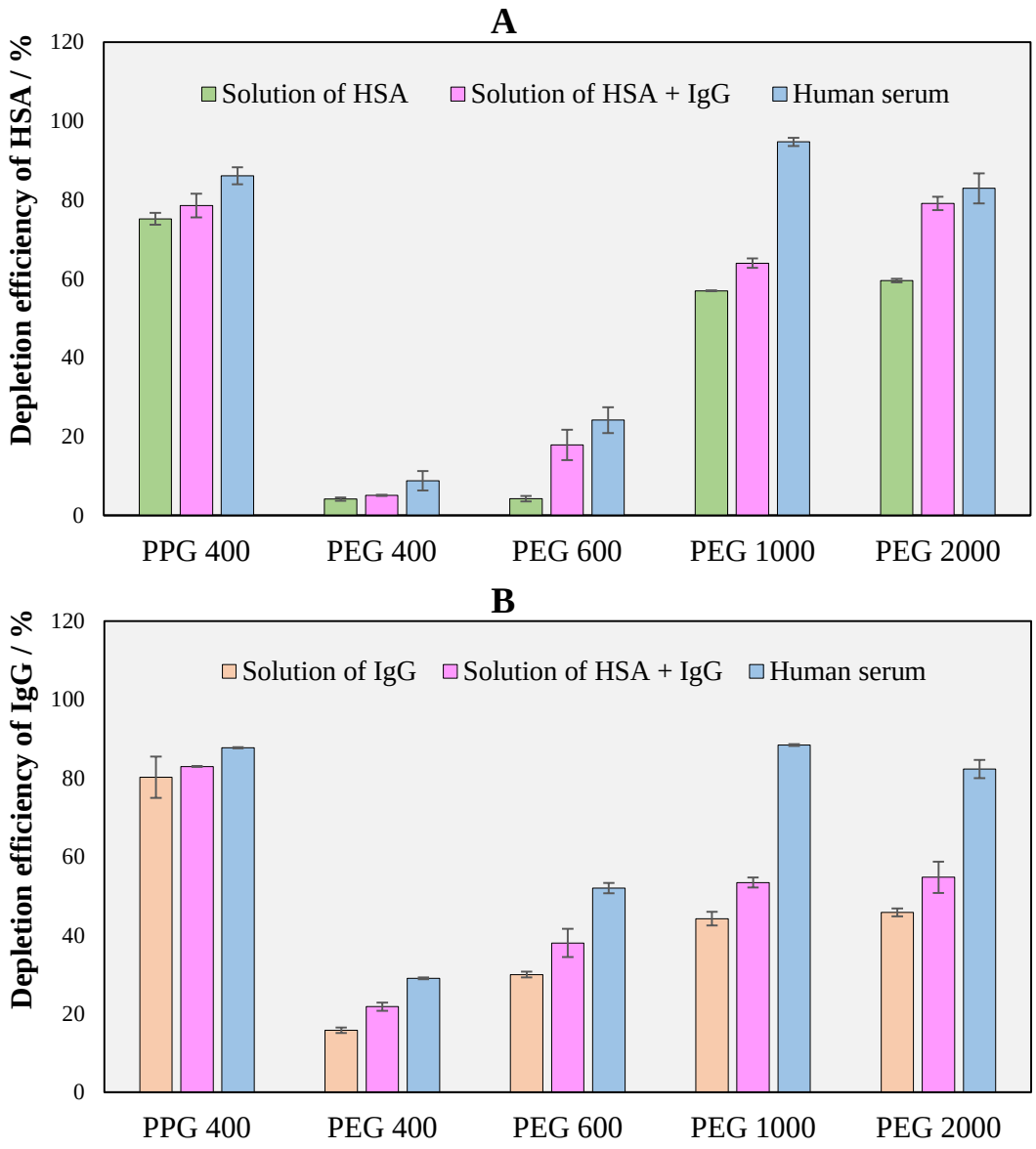

Figure 3.6. Depletion efficiencies obtained for (A) HSA and (B) IgG in TPP formed by 30 wt% of homopolymer, 30 wt% of $K_3C_6H_5O_7/C_6H_8O_7$ with: solution of HSA (■), solution of IgG (■), solution of HSA + IgG (■) and solution of human serum (■).

According to Figure 3.5, it is possible to observe, for all the different homopolymers, that the systems with only HSA and only IgG, represented by green and orange bars, respectively, are the ones presenting lower depletion efficiencies, followed by the ones with solution of HSA + IgG (pink bars). The systems containing the complex solution of human serum, represented by blue bars, are the ones displaying higher depletion efficiencies in all cases.

In the TPP formed by PPG 400 and citrate buffered salt, depletion efficiencies ranging between 75% and 87% were achieved with all solutions. The similar depletion

efficiencies here obtained with different protein compositions indicate that this polymer is efficient for protein depletion, resultant from its highly hydrophobic nature; however, sample complexity does not seem to have a significant impact in the precipitation of these two proteins at the interphase. Regarding the TPP formulated using PEGs of different molecular weights, it was observed that in all systems higher depletions of both HSA and IgG were reached with serum, and the efficiency of these systems to deplete these proteins decreased with the reduction of sample complexity.

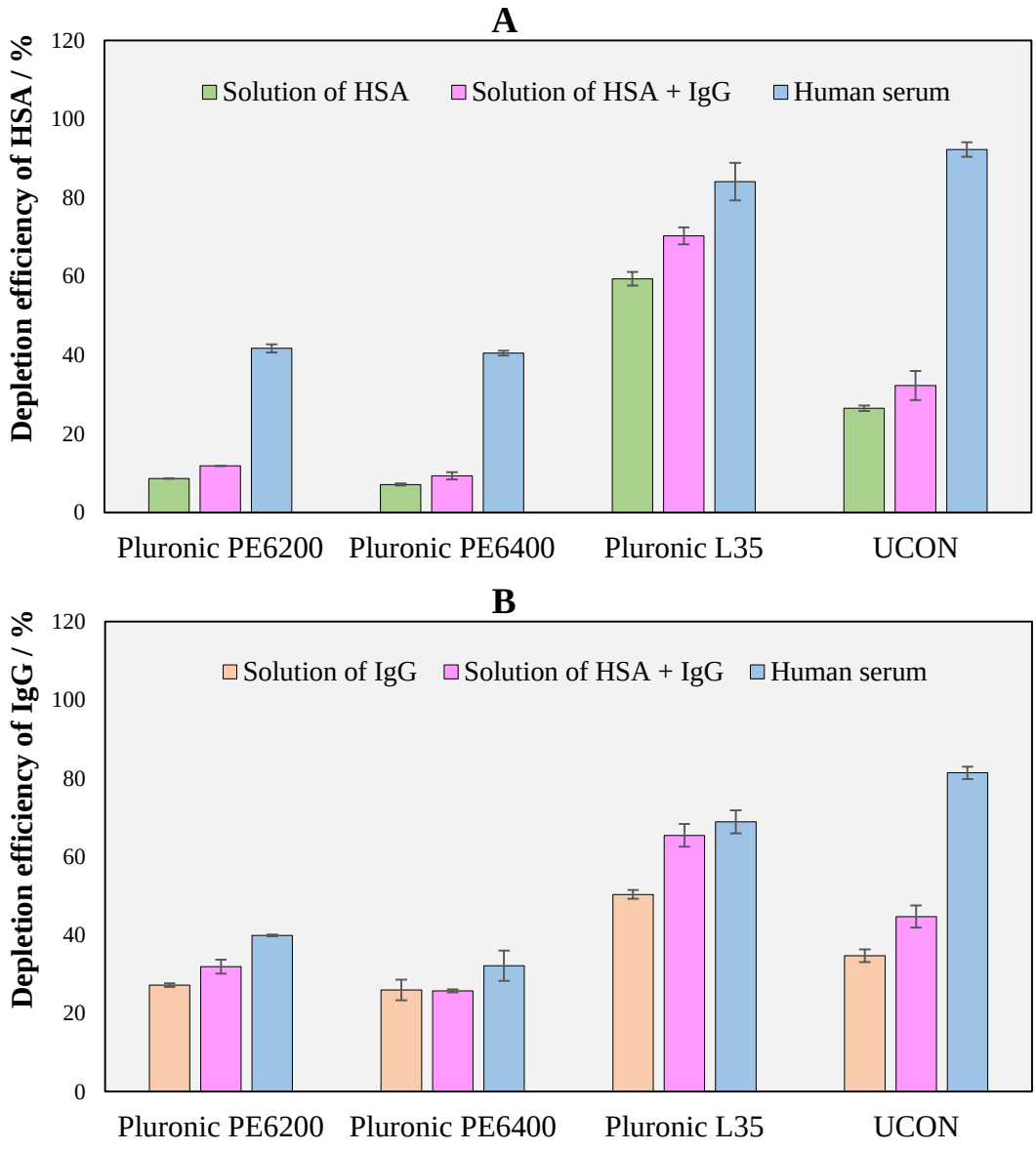

Figure 3.7. Depletion efficiencies obtained for (A) HSA and (B) IgG in TPP formed by 30 wt% of copolymer, 30 wt% of $K_3C_6H_5O_7/C_6H_8O_7$ and solution of HSA (■), solution of IgG (■), solution of HSA + IgG (■) and solution of human serum (■).

As shown in Figure 3.6, among the different copolymers studied it was verified that in all the cases the systems with serum presented higher depletion efficiencies, followed by the ones with solution of HSA and IgG, with the systems containing the aqueous solutions containing only HSA and only IgG displaying the lower depletion efficiencies.

TPP comprising Pluronic L35 and UCON reported the higher depletion efficiencies among the copolymers studied. The systems composed of Pluronic L35 presented higher depletion efficiencies than UCON for the solution of HSA, solution of IgG and solution of HSA + IgG. However, when dealing with the more complex samples human serum, the UCON-based TPP outpaced the ability of Pluronic L35 to deplete HSA and IgG.

The systems formulated using the Pluronics PE6200 and PE6400 were the ones presenting lower ability to deplete HSA and IgG, with the different samples analyzed. In these systems although some of HSA and IgG content precipitated in the interphase, both proteins migrated preferentially to the copolymer-rich phase (top phase). Also, it was observed that independently of sample complexity the top phases of these TPP were very viscous making it difficult to separate the phases. After all considerations made so far, the copolymers Pluronic PE6200 and Pluronic PE6400 were not selected to extract the biomarker PTX-3.

3.4. EXTRACTION OF PTX-3 USING TPP

After addressing the most promising TPP for the pretreatment of human serum samples, these systems were then evaluated in terms of their ability to extract the lung cancer biomarker PTX-3 in a single-step. The ABS/TPP selected were the ones formulated using the homopolymers PEG 1000, PEG 2000 and PPG 400, and the copolymers UCON and Pluronic L35. ABS with only aqueous solution of PTX-3 were first prepared in order to elucidate the partition behavior of this protein between the two phases, where a complete partition of PTX-3 to the top phase was accomplished in all systems. In these systems no precipitation of the protein was observed. The extraction efficiencies of PTX-3 obtained are given in Table A6, in the Appendix.

The recovery yield of PTX-3 in each phase of the different ABS/TPP with human serum spiked with PTX-3 studied is represented in Figure 3.7, whose detailed results are given in Table A7, in the Appendix.

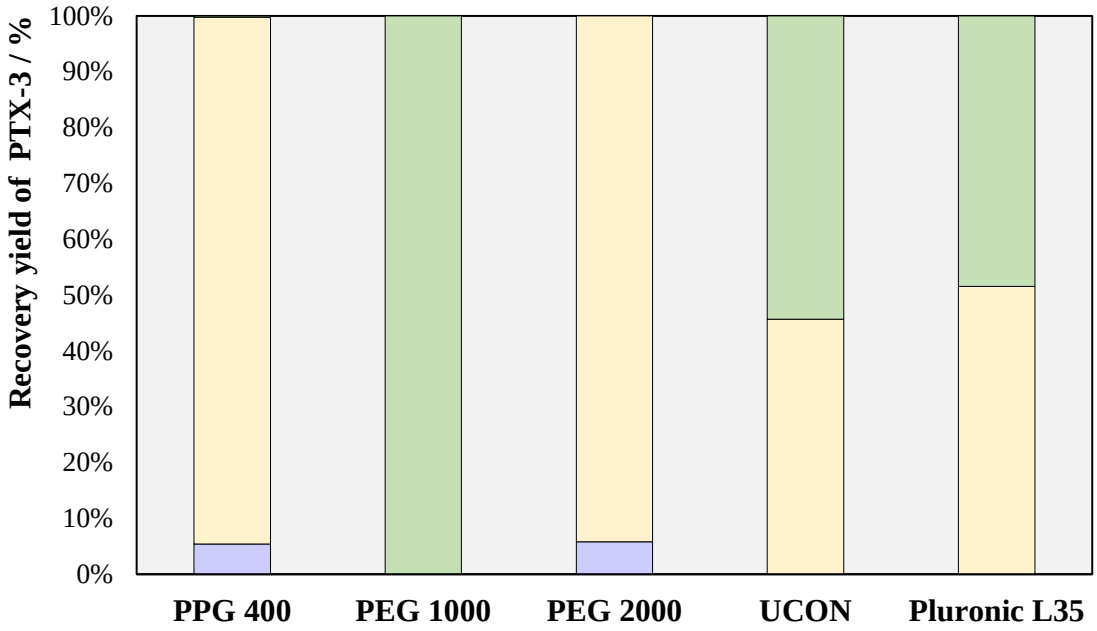

Figure 3.8. Recovery yield of PTX-3 in the top phase (■), interphase (■) and bottom phase (■), in the TPP formed by 30 wt% of homopolymer/copolymer and 30 wt% of $K_3C_6H_5O_7/C_6H_8O_7$ buffer (pH = 7), at 25ºC and atmospheric pressure.

For the five studied ABS/TPP with spiked human serum, extraction efficiencies of PTX-3 to the polymer-rich phase ranging from 0 to 100% were obtained in a single step. The system composed of PEG 1000 allowed a complete partition of PTX-3 toward the homopolymer-rich phase, with no PTX-3 being quantified in the salt-rich phase and interphase. The partitioning results obtained with UCON and Pluronic L35 indicate that circa half of the PTX-3 content precipitated at the interphase, with the remaining proteins migrating to the top phase. In these TPP formulated using copolymers, no PTX-3 was quantified in the bottom phase. Lastly, in the systems composed of the homopolymers PPG 400 and PEG 2000, almost all the content of PTX-3 precipitated at the interphase and no PTX-3 was found in the homopolymer-rich phase. Since the aim was to promote the partitioning of PTX-3 to the top phase, the results obtained for these two last systems made them unsuitable. Overall, the ABS/TPP formed by PEG 100 allows the complete extraction of PTX-3 in the PEG-rich phase, with no losses of the biomarker, with the simultaneous and complete depletion of IgG and HSA.

The values of PTX-3 quantified in a sample of pretreated human using ABS/TPP and in a sample non treated are reported in Table 3.4, as well as their percentage relative

error in relation to the added value and known amount of PTX-3 in each sample (250 pg), allowing to evaluate the accuracy of each assay in the quantification of PTX-3.

Table 3.4. Values of PTX-3 quantified in a pretreated sample with ABS/TPP and in a sample non treated of human serum, and their percentage relative errors to the real amount of PTX-3 added.

Human serum	PTX-3 / pg	Relative error / %
Sample pretreated	252.1 ± 4.7	0.8
Sample non treated	320.1 ± 7.5	28.1

According to the data provided in Table 3.4, the PTX-3 quantified in the pretreated sample presents a low relative error, namely 0.8%, whereas the non-treated human serum led to a relative error of 28.1% in the PTX-3 quantification. These results confirm that the pretreatment of human serum using ABS/TPP reduces the interference of the abundant proteins HSA and IgG in the quantification of PTX-3 in human serum samples, therefore leading to more accurate results.

In summary, between all the systems studied, the TPP formulated with PEG 1000 was the most promising one, allowing the complete extraction of PTX-3 in the polymer-rich phase, in a single step. The results here obtained together with the elevated depletion efficiencies reported for HSA and IgG previously discussed, indicate that polymer based TPP can be applied as an alternative pretreatment technique for human serum, particularly useful for lung cancer diagnosis and prognosis through the extraction of biomarkers.

IV – CONCLUSIONS

4.1. CONCLUDING REMARKS

Novel aqueous biphasic systems composed of homopolymers/copolymers and a citrate buffered salt were evaluated in terms of their performance as a pretreatment strategy of human serum to deplete the most abundant proteins HSA and IgG and extract the lung cancer biomarker PTX-3, in a single step. The ABS phase diagrams and tie-lines were determined to infer mixture compositions required to form systems with two coexisting phases that can be used both as a depletion and extraction tools. The depletion of HSA and IgG was then performed using the systems previously optimized. Depletion efficiencies above 80% were obtained for both proteins in the TPP composed of the homopolymers PEG 1000, PEG 2000 and PPG 400, and the copolymers Pluronic L35 and UCON. These systems were then applied in the extraction of PTX-3 to the polymer-rich phase. Promising results were obtained with the TPP system composed of PEG 1000, with extraction efficiencies of PTX-3 of 100%, while keeping the complete depletion performance for HSA and IgG. The comparison between the values of PTX-3 quantified in a sample pretreated and in a sample non treated confirmed that the pretreatment of human serum using ABS/TPP leads to more accurate results. Finally, according to the results achieved in this work, polymer-based TPP can be used as a cost-effective alternative for the pretreatment of complex samples, such as human serum, reducing the interference of the most abundant proteins and consequently allowing the quantification of cancer biomarkers.

4.2. FUTURE WORK

This work displayed promising results for a future application of ABS/TPP composed of polymers and salts to pretreat biological samples for a more accurate lung cancer diagnosis and prognosis. However, to completely achieve this goal, future work needs to be performed, including the following steps:

-To validate the use of the ABS/TPP strategies to simultaneously deplete HSA and IgG and extract PTX-3 from real human serum samples from lung cancer patients, including approved cohorts;

-To extend the use of the TPP-ABS to other lung cancer biomarkers, envisioning a differential and more accurate diagnosis:

-To proceed with the regulatory framework required to register a novel pretreatment strategy related with cancer prognosis and diagnosis.

In addition to these goals, the results here obtained pave the way for the evaluation of these systems for the pretreatment of other biological fluids, such as urine and saliva, for diagnosis purpose. Furthermore, it is of high relevance to expand the use of the systems here developed for the extraction of other metabolites and diagnosis of other pathologies.

V – REFERENCES

1 F. Bray, J. Ferlay, I. Soerjomataram, R. L. Siegel, L. A. Torre and A. Jemal, *CA. Cancer J. Clin.*, 2018, **68**, 394–424.

2 P. Goldstraw, J. Crowley, K. Chansky, D. J. Giroux, P. A. Groome, R. Rami-Porta, P. E. Postmus, V. Rusch and L. Sobin, *J. Thorac. Oncol.*, 2007, **2**, 706–714.

3 R. Etzioni, N. Urban, S. Ramsey, M. McIntosh, S. Schwartz, B. Reid, J. Radich, G. Anderson and L. Hartwell, *Nat. Rev. Cancer*, 2003, **3**, 243–252.

4 J. A. Ludwig and J. N. Weinstein, *Nat. Rev. Cancer*, 2005, **5**, 845–856.

5 N. L. Henry and D. F. Hayes, *Mol. Oncol.*, 2012, **6**, 140–146.

6 I. Ghosh, D. Bhattacharjee, A. K. Das, G. Chakrabarti, A. Dasgupta and S. K. Dey, *Indian J. Clin. Biochem.*, 2013, **28**, 24–29.

7 E. P. Diamandis, L. Goodglick, C. Planque and M. D. Thornquist, *Clin. Cancer Res.*, 2011, **17**, 2395–2399.

8 B. Domon and R. Aebersold, *Mol. Cell. Proteomics*, 2006, **5**, 1921–1926.

9 N. L. Anderson and N. G. Anderson, *Nature*, 2002, 1, 845–867.

10 K. Chandramouli and P.-Y. Qian, *Hum. Genomics Proteomics*, 2009, **1**, 1–22.

11 J. Xiao, T. Wang, P. Li, R. Liu, Q. Li and K. Bi, *J. Chromatogr. B Anal. Technol. Biomed. Life Sci.*, 2016, **1028**, 33–41.

12 M. Selvadurai and S. N. Meyyanathan, *Pharm. Methods*, 2011, **2**, 106–111.

13 V. Ferrone, M. Carlucci, P. Palumbo and G. Carlucci, *J. Pharm. Biomed. Anal.*, 2016, **123**, 205–212.

14 A. Dubala, J. S. K. Nagarajan, C. S. Vimal and R. George, *J. Chromatogr. B Anal. Technol. Biomed. Life Sci.*, 2013, **921**, 49–55.

15 S. A. Mohammed, M. S. Eissa and H. M. Ahmed, *J. Chromatogr. B Anal. Technol. Biomed. Life Sci.*, 2017, **1043**, 235–240.

16 C. Polson, P. Sarkar, B. Incledon, V. Raguvaran and R. Grant, *J. Chromatogr. B Anal. Technol. Biomed. Life Sci.*, 2003, **785**, 263–275.

17 M. Rawa-Adkonis, L. Wolska, A. Przyjazny and J. Namieśnik, *Anal. Lett.*, 2006, **39**, 2317–2331.

18 M.-C. Hennion, *Haematologica*, 2006, **91**, 1027–1032.

19 Z. Ning, B. Hawley, D. Seebun and D. Figeys, *J. Membr. Biol.*, 2014, **247**, 941–947.

20 M. Iqbal, Y. Tao, S. Xie, Y. Zhu, D. Chen, X. Wang, L. Huang, D. Peng, A. Sattar, M. A. B. Shabbir, H. I. Hussain, S. Ahmed and Z. Yuan, *Biol. Proced. Online*, 2016, **18**, 1–18.

21 P.-Å. Albertsson, *Nature*, 1958, **182**, 709–711.

22 M. M. Pereira, J. D. Calixto, A. C. A. Sousa, B. J. Pereira, Á. S. Lima, J. A. P. Coutinho and M. G. Freire, *Sci. Rep.*, 2020, **10**, 1–8.

23 B. H. Han, S. Kim, G. Seo, Y. Heo, S. Chung and J. Y. Kang, *Lab Chip*, 2020, **20**, 3552–3559.

24 H. Shin, Y. H. Park, Y. G. Kim, J. Y. Lee and J. Park, *PLoS One*, 2018, **13**, 1–15.

25 Y. H. Park, H. W. Shin, A. R. Jung, O. S. Kwon, Y. J. Choi, J. Park and J. Y. Lee, *Sci. Rep.*, 2016, **6**, 1–9.

26 M. Pereira, 2017, University of Aveiro, Portugal.

27 R. L. Siegel, K. D. Miller and A. Jemal, *CA. Cancer J. Clin.*, 2019, **69**, 7–34.

28 A. Pérez, E. K. Santamaria and D. Operario, *Cancer Lett.*, 2017, **5**, 1–8.

29 J. A. Barta, C. A. Powell and J. P. Wisnivesky, *Ann. Glob. Heal.*, 2019, **85**, 1–16.

30 M. Naghavi, *JAMA Oncol.*, 2013, **1**, 505–527.

31 R. Luengo-Fernandez, J. Leal, A. Gray and R. Sullivan, *Lancet Oncol.*, 2013, **14**, 1165–1174.

32 Nowell P. C., *Science (80-.).*, 1976, **194**, 23–28.

33 D. Hanahan and R. A. Weinberg, *Cell Press*, 2000, **100**, 57–70.

34 D. Hanahan and R. A. Weinberg, *Cell*, 2011, **144**, 18–30.

35 G. Evan, S. Lowe and E. Cepero, *Nature*, 2004, **432**, 1–9.

36 J. M. Adams and S. Cory, *Oncogene*, 2007, **26**, 1324–1337.

37 G. Evan and T. Littlewood, *Science (80-.).*, 1998, **281**, 1317–1322.

38 D. Hanahan and J. Folkman, *Cell*, 1996, **86**, 353–364.

39 James E Talmadge and Isaiah J Fidler, *Cancer Res.*, 2010, **70**, 5649–5669.

40 I. J. Fidler, *Nat. Rev. Cancer*, 2002, **3**, 46–56.

41 R. Kim, M. Emi and K. Tanabe, *Immunology*, 2007, **121**, 1–14.

42 A. J. Alberg, M. V. Brock, J. G. Ford, J. M. Samet and S. D. Spivack, *Chest*, 2013, **143**, 1–29.

43 H. Graham, *Soc. Sci. Med.*, 1996, **43**, 243–254.

44 R. Doll, R. Peto, J. Boreham and I. Sutherland, *Br. Med. J.*, 2004, **328**, 1519–1528.

45 R. Peto, J. Boreham, A. D. Lopez, M. Thun and C. Heath, *Lancet*, 1992, **339**, 1268–1278.

46 J. E. Bailey-Wilson, C. I. Amos, S. M. Pinney, G. M. Petersen, M. De Andrade, J. S. Wiest, P. Fain, A. G. Schwartz, M. You, W. Franklin, C. Klein, A. Gazdar, H. Rothschild, D. Mandal, T. Coons, J. Slusser, J. Lee, C. Gaba, E. Kupert, A. Perez, X. Zhou, D. Zeng, Q. Liu, Q. Zhang, D. Seminara, J. Minna and M. W. Anderson, *Am. J. Hum. Genet.*, 2004, **75**, 460–474.

47 J. Lissowska, A. Bardin-Mikolajczak, T. Fletcher, D. Zaridze, N. Szeszenia-Dabrowska, P. Rudnai, E. Fabianova, A. Cassidy, D. Mates, I. Holcatova, V. Vitova, V. Janout, A. A. T. Mannetje, P. Brennan and P. Boffetta, *Am. J. Epidemiol.*, 2005, **162**, 326–333.

48 IARC Working Group on the Evaluation of Carcinogenic Risks to Humans, *Eval. Carcinog. RISKS TO HUMANS Ioniz. Radiation, Part 1 X- Gamma (γ)-Radiation, Neutrons*, 2000, pp 508.

49 V. J. Cogliano, R. Baan, K. Straif, Y. Grosse, B. Lauby-Secretan, F. El Ghissassi, V. Bouvard, L. Benbrahim-Tallaa, N. Guha, C. Freeman, L. Galichet and C. P. Wild, *J. Natl. Cancer Inst.*, 2010, **103**, 1827–1839.

50 G. Cannon, *Choice Rev. Online*, 2008, **45**, 45-5024-45–5024.

51 R. C. Brownson and M. C. R. Alavanja, *Cancer Causes Control*, 2000, **11**, 853–858.

52 S. T. Mayne, J. Buenconsejo and D. T. Janerich, *Am. J. Epidemiol.*, 1999, **149**, 13–20.

53 Y. -T Gao, W. J. Blot and W. Zheng, *Int. J. Cancer*, 1987, **40**, 604–609.

54 R. Wood, G. Taylor-Stokes, M. Lees and O. Chirita, *Value Heal.*, 2017, **20**, A427.

55 G. Gibson, R. Loddenkemper and Y. Sibille, *Eur. Respir. Soc.*, 2013, **1**, 16–27.

56 G. Pelosi, A. Sonzogni, S. Harari, A. Albini, E. Bresaola, C. Marchiò, F. Massa, L. Righi, G. Gatti, N. Papanikolaou, N. Vijayvergia, F. Calabrese and M. Papotti, *Transl. Lung Cancer Res.*, 2017, **6**, 513–529.

57 K. Inamura, *Front. Oncol.*, 2017, **7**, 1–7.

58 T. N. Zamay, G. S. Zamay, O. S. Kolovskaya, R. A. Zukov, M. M. Petrova, A. Gargaun, M. V.

Berezovski and A. S. Kichkailo, *Cancers (Basel).*, 2017, **9**, 1–22.

59 K. M. Muller, *Eur. J. Respir. Dis.*, 1984, **65**, 4–19.

60 W. D. Travis, *Mod. Pathol.*, 2012, **25**, 18–30.

61 J. D. M. Jill E. Larsen, *J. Thorac. Dis.*, 2011, **5**, 703–740.

62 W. A. Cooper, D. C. L. Lam, S. A. O'Toole and J. D. Minna, *J. Thorac. Dis.*, 2013, **5**, 479–490.

63 J. H. Schiller, *Oncology*, 2001, **61**, 3–13.

64 H. M. Marshall, R. V. Bowman, I. A. Yang, K. M. Fong and C. D. Berg, *J. Thorac. Dis.*, 2013, **5**, 524–539.

65 R. Mayeux, *NeuroRx*, 2004, **1**, 182–188.

66 R. Fuchsova, O. Topolcan, J. Windrichova, M. Hora, O. Dolejsova, L. Pecen, P. Kasik, J. Novak, M. Casova and J. Smejkal, *Anticancer Res.*, 2015, **35**, 4855–4858.

67 T. Shpitzer, Y. Hamzany, G. Bahar, R. Feinmesser, D. Savulescu, I. Borovoi, M. Gavish and R. M. Nagler, *Br. J. Cancer*, 2009, **101**, 1194–1198.

68 T. DeVos, R. Tetzner, F. Model, G. Weiss, M. Schuster, J. Distler, K. V. Steiger, R. Grützmann, C. Pilarsky, J. K. Habermann, P. R. Fleshner, B. M. Oubre, R. Day, A. Z. Sledziewski and C. Lofton-Day, *Clin. Chem.*, 2009, **55**, 1337–1346.

69 S.-J. Dawson, D. W. Y. Tsui, M. Murtaza, H. Biggs, O. M. Rueda, S.-F. Chin, M. J. Dunning, D. Gale, T. Forshew, B. Mahler-Araujo, S. Rajan, S. Humphray, J. Becq, D. Halsall, M. Wallis, D. Bentley, C. Caldas and N. Rosenfeld, *N. Engl. J. Med.*, 2013, **368**, 1199–1209.

70 M. V. Brock, C. M. Hooker, E. Ota-Machida, Y. Han, M. Guo, S. Ames, S. Glöckner, S. Piantadosi, E. Gabrielson, G. Pridham, K. Pelosky, S. A. Belinsky, S. C. Yang, S. B. Baylin and J. G. Herman, *N. Engl. J. Med.*, 2008, **358**, 1118–1128.

71 X. Chen, Y. Ba, L. Ma, X. Cai, Y. Yin, K. Wang, J. Guo, Y. Zhang, J. Chen, X. Guo, Q. Li, X. Li, W. Wang, Y. Zhang, J. Wang, X. Jiang, Y. Xiang, C. Xu, P. Zheng, J. Zhang, R. Li, H. Zhang, X. Shang, T. Gong, G. Ning, J. Wang, K. Zen, J. Zhang and C. Y. Zhang, *Cell Res.*, 2008, **18**, 997–1006.

72 E. Jantus-Lewintre, M. Usó, E. Sanmartín and C. Camps, *Lung Cancer Targets Ther.*, 2012, **3**, 21–29.

73 S. Nagrath, L. V. Sequist, S. Maheswaran, D. W. Bell, D. Irimia, L. Ulkus, M. R. Smith, E. L. Kwak, S. Digumarthy, A. Muzikansky, P. Ryan, U. J. Balis, R. G. Tompkins, D. A. Haber and M. Toner, *Nature*, 2007, **450**, 1235–1239.

74 G. Sozzi, D. Conte, M. E. Leon, R. Cirincione, L. Roz, C. Ratcliffe, E. Roz, N. Cirenei, M. Bellomi, G. Pelosi, M. A. Pierotti and U. Pastorino, *J. Clin. Oncol.*, 2003, **21**, 3902–3908.

75 N. Carlomagno, P. Incollingo, V. Tammaro, G. Peluso, N. Rupealta, G. Chiacchio, M. L. Sandoval Sotelo, G. Minieri, A. Pisani, E. Riccio, M. Sabbatini, U. M. Bracale, A. Calogero, C. A. Dodaro and M. Santangelo, *Biomed Res. Int.*, 2017, **17**, 1–11.

76 T. N. England, 2001, **344**, 783–792.

77 E. H. Romond, E. A. Perez, J. Bryant, V. J. Suman, C. E. Geyer, N. E. Davidson, E. Tan-Chiu, S. Martino, S. Paik, P. A. Kaufman, S. M. Swain, T. M. Pisansky, L. Fehrenbacher, L. A. Kutteh, V. G. Vogel, D. W. Visscher, G. Yothers, R. B. Jenkins, A. M. Brown, S. R. Dakhil, E. P. Mamounas, W. L. Lingle, P. M. Klein, J. N. Ingle and N. Wolmark, *N. Engl. J. Med.*, 2005, **353**, 1673–1684.

78 E. Pisano, C. Gatsonis, R. Boineau, M. Domanski, C. Troutman, J. Anderson, G. Johnson, S. E. Mcnulty, N. Clapp-channing, L. D. Davidson-ray, E. S. Fraulo, D. P. Fishbein and R. M. Luceri, *Massachusetts Med. Soc.*, 2005, **353**, 225–237.

79 W. R. Miller, T. J. Anderson, J. M. Dixon and P. T. K. Saunders, *Br. J. Cancer*, 2006, **94**, 1333–1338.

80 R. D. Mass, M. F. Press, S. Anderson, M. A. Cobleigh, C. L. Vogel, N. Dybdal, G. Leiberman, D. J. Slamon and V. E. Paton, *Clin. Breast Cancer*, 2005, **6**, 240–246.

81 W. J. Catalona, D. S. Smith, T. L. Ratliff, K. M. Dodds, D. E. Coplen, J. J. J. Yuan, J. A. Petros and G. L. Andriole, *N. Engl. J. Med.*, 2005, **329**, 783–792.

82 T. Chakrabortty, C. R. Murthy and M. Varma, *arXiv*, 2019, **41**, 1–13.

83 H. Lee, J. E. Park and J. M. Nam, *Nat. Commun.*, 2014, **5**, 3367.

84 H. Shintaku, J. W. Palko, G. M. Sanders and J. G. Santiago, *Angew. Chemie*, 2014, **126**, 14033–14036.

85 R. De La Rica and M. M. Stevens, *Nat. Nanotechnol.*, 2012, **7**, 821–824.

86 W. C. Law, K. T. Yong, A. Baev and P. N. Prasad, *ACS Nano*, 2011, **5**, 4858–4864.

87 J.-A. L. Kelsey C. Martin Mhatre V. Ho, *Bone*, 2012, **23**, 1–7.

88 S. R. Panikkanvalappil, M. A. MacKey and M. A. El-Sayed, *J. Am. Chem. Soc.*, 2013, **135**, 4815–4821.

89 M. Li, S. K. Cushing, J. Zhang, S. Suri, R. Evans, W. P. Petros, L. F. Gibson, D. Ma, Y. Liu and N. Wu, *ACS Nano*, 2013, **7**, 4967–4976.

90 M. M. Varma, H. D. Inerowicz, F. E. Regnier and D. D. Nolte, *Biosens. Bioelectron.*, 2004, **19**, 1371–1376.

91 S. Rana, A. K. Singla, A. Bajaj, S. G. Elci, O. R. Miranda, R. Mout, B. Yan, F. R. Jirik and V. M. Rotello, *ACS Nano*, 2012, **6**, 8233–8240.

92 K. Mizusawa, Y. Takaoka and I. Hamachi, *J. Am. Chem. Soc.*, 2012, **134**, 13386–13395.

93 J. Wang, L. Wu, J. Ren and X. Qu, *Small*, 2012, **8**, 259–264.

94 Y. Song, W. Wei and X. Qu, *Adv. Mater.*, 2011, **23**, 4215–4236.

95 M. Labib, N. Khan, S. M. Ghobadloo, J. Cheng, J. P. Pezacki and M. V. Berezovski, *J. Am. Chem. Soc.*, 2013, **135**, 3027–3038.

96 B. V. Chikkaveeraiah, A. A. Bhirde, N. Y. Morgan, H. S. Eden and X. Chen, *ACS Nano*, 2012, **6**, 6546–6561.

97 R. C. Zangar, D. S. Daly and A. M. White, *Expert Rev. Proteomics*, 2006, **3**, 37–44.

98 K. A. Ruiz-Ceja and Y. I. Chirino, *Biomed. Pharmacother.*, 2017, **90**, 24–37.

99 B. M. Nolen, A. Lomakin, A. Marrangoni, L. Velikokhatnaya, D. Prosser and A. E. Lokshin, *Cancer Prev. Res.*, 2015, **8**, 111–119.

100 X. Zhang, M. Guo, J. Fan, Z. Lv, Q. Huang, J. Han, F. Wu, G. Hu, J. Xu and Y. Jin, *Cancer Biomarkers*, 2016, **16**, 415–423.

101 X. Hu, W. Huang, F. Wang, Y. Dai, X. Hu, D. Yue and S. Wang, *Medicine (Baltimore).*, 2020, **99**, e21254.

102 H. J. Oh, H. Y. Park, K. H. Kim, C. K. Park, H. J. Shin, J. H. Lim, Y. S. Kwon, I. J. Oh, Y. Il Kim, S. C. Lim, Y. C. Kim, S. H. Kim and M. G. Shin, *J. Thorac. Dis.*, 2016, **8**, 2530–2537.

103 C. Liu, Y. Yao and W. Wang, *Med. Oncol.*, 2014, **31**, 1–6.

104 M. Grunnet and J. B. Sorensen, *Lung Cancer*, 2012, **76**, 138–143.

105 K. Okamura, K. Takayama, M. Izumi, T. Harada, K. Furuyama and Y. Nakanishi, *Lung Cancer*, 2013, **80**, 45–49.

106 E. F. Patz, M. J. Campa, E. B. Gottlin, I. Kusmartseva, R. G. Xiang and J. E. Herndon, *J. Clin. Oncol.*, 2007, **25**, 5578–5583.

107 A. El Bastawisy, M. El Azzouny, G. Mohammed, A. A. Allah and E. Behiry, *Ecancermedicalscience*, 2014, **8**, 1–9.

108 C. de Jong, V. H. M. Deneer, J. C. Kelder, H. Ruven, T. C. G. Egberts and G. J. M. Herder, *Thorac. Cancer*, 2020, **11**, 1790–1800.

109 M. G. Dal Bello, R. A. Filiberti, A. Alama, A. M. Orengo, M. Mussap, S. Coco, I. Vanni, S. Boccardo, E. Rijavec, C. Genova, F. Biello, G. Barletta, G. Rossi, M. Tagliamento, C. Maggioni and F. Grossi, *J. Transl. Med.*, 2019, **17**, 1–10.

110 B. M. Nolen, A. Lomakin, A. Marrangoni, L. Velikokhatnaya, D. Prosser, A. E. Lokshin, M. A. Isgrò, P. Bottoni and R. Scatena, *Adv. Exp. Med. Biol.*, 2015, **8**, 111–119.

111 K. Kagohashi, H. Satoh, K. Kurishima, K. Kadono, H. Ishikawa, M. Ohtsuka and K. Sekizawa, *Lung*, 2008, **186**, 323–326.

112 E. Wojcik and J. K. Kulpa, *Lung Cancer Targets Ther.*, 2017, **8**, 231–240.

113 H. Gewurz, X. H. Zhang and T. F. Lint, *Curr. Opin. Immunol.*, 1995, **7**, 54–64.

114 A. P. Osmand, B. Friedenson, H. Gewurz, R. H. Painter, T. Hofmann and E. Shelton, *Proc. Natl. Acad. Sci. U. S. A.*, 1977, **74**, 739–743.

115 L. Deban, B. Bottazzi, C. Garlanda, Y. M. De La Torre and A. Mantovani, *BioFactors*, 2009, **35**, 138–145.

116 A. Agrawal, P. P. Singh, B. Bottazzi, C. Garlanda and A. Mantovani, *Adv. Exp. Med. Biol.*, 2009, **653**, 98–116.

117 F. Breviario, E. M. Aniello, J. Golay, G. Peri, B. Bottazzi, A. Bairoch, S. Saccone, R. Marzella, V. Predazzi, M. Rocchi, G. Della Valle, E. Dejana, A. Mantovani and M. Introna, *J. Biol. Chem.*, 1992, **267**, 22190–22197.

118 C. Garlanda, B. Bottazzi, A. Bastone and A. Mantovani, *Annu. Rev. Immunol.*, 2005, **23**, 337–366.

119 B. Bottazzi, C. Garlanda, G. Salvatori, P. Jeannin, A. Manfredi and A. Mantovani, *Curr. Opin. Immunol.*, 2006, **18**, 10–15.

120 P. Jeannin, B. Bottazzi, M. Sironi, A. Doni, M. Rusnati, M. Presta, V. Maina, G. Magistrelli, J. F. Haeuw, G. Hoeffel, N. Thieblemont, N. Corvaia, C. Garlanda, Y. Delneste and A. Mantovani, *Immunity*, 2005, **22**, 551–560.

121 A. J. Nauta, B. Bottazzi, A. Mantovani, G. Salvatori, U. Kishore, W. J. Schwaeble, A. R. Gingras, S. Tzima, F. Vivanco, J. Egido, O. Tijsma, E. C. Hack, M. R. Daha and A. Roos, *Eur. J. Immunol.*, 2003, **33**, 465–473.

122 G. D. Norata, P. Marchesi, A. Pirillo, P. Uboldi, G. Chiesa, V. Maina, C. Garlanda, A. Mantovani and A. L. Catapano, *Arterioscler. Thromb. Vasc. Biol.*, 2008, **28**, 925–931.

123 A. Doni, G. Peri, M. Chieppa, P. Allavena, F. Pasqualini, L. Vago, L. Romani, C. Garlanda and A. Mantovani, *Eur. J. Immunol.*, 2003, **33**, 2886–2893.

124 C. C. Dos Santos, B. Han, C. F. Andrade, X. Bai, S. Uhlig, R. Hubmayr, M. Tsang, M. Lodyga, S. Keshavjee, A. S. Slutsky and M. Liu, *Physiol. Genomics*, 2005, **19**, 331–342.

125 A. J. Nauta, S. De Haij, B. Bottazzi, A. Mantovani, M. C. Borrias, J. Aten, M. P. Rastaldi, M. R. Daha, C. Van Kooten and A. Roos, *Kidney Int.*, 2005, **67**, 543–553.

126 S. Jaillon, G. Peri, Y. Delneste, I. Frémaux, A. Doni, F. Moalli, C. Garlanda, L. Romani, H. Gascan, S. Bellocchio, S. Bozza, M. A. Cassatella, P. Jeannin and A. Mantovani, *J. Exp. Med.*, 2007, **204**, 793–804.

127 N. Polentarutti, B. Bottazzi, E. Di Santo, E. Blasi, D. Agnello, P. Ghezzi, M. Introna, T. Bartfai, G. Richards and A. Mantovani, *J. Neuroimmunol.*, 2000, **106**, 87–94.

128 A. R. Goodman, D. E. Levy, L. F. L. Reis and J. Vilcek, *J. Leukoc. Biol.*, 2000, **67**, 387–395.

129 A. Abderrahim-Ferkoune, O. Bezy, C. Chiellini, M. Maffei, P. Grimaldi, F. Bonino, N. Moustaid-Moussa, F. Pasqualini, A. Mantovani, G. Ailhaud and E. Z. Amri, *J. Lipid Res.*, 2003, **44**, 994–1000.

130 M. Klouche, G. Peri, C. Knabbe, H. H. Eckstein, F. X. Schmid, G. Schmitz and A. Mantovani, *Atherosclerosis*, 2004, **175**, 221–228.

131 A. Mantovani, C. Garlanda, A. Doni and B. Bottazzi, *J. Clin. Immunol.*, 2008, **28**, 1–13.

132 A. Mantovani, P. Allavena, A. Sica and F. Balkwill, *Nature*, 2008, **454**, 436–444.

133 S. Kondo, H. Ueno, H. Hosoi, J. Hashimoto, C. Morizane, F. Koizumi, K. Tamura and T. Okusaka, *Br. J. Cancer*, 2013, **109**, 739–746.

134 B. Choi, E. J. Lee, Y. S. Park, S. M. Kim, E. Y. Kim, Y. Song, S. W. Kang, M. H. Rhu and E. J. Chang, *Anticancer Res.*, 2015, **35**, 2663–2668.

135 T. Barbui, A. Carobbio, G. Finazzi, A. M. Vannucchi, G. Barosi, E. Antonioli, P. Guglielmelli, A. Pancrazzi, S. Salmoiraghi, P. Zilio, C. Ottomano, R. Marchioli, I. Cuccovillo, B. Bottazzi, A. Mantovani and A. Rambaldi, *Haematologica*, 2011, **96**, 315–318.

136 C. Planque, V. Kulasingam, C. R. Smith, K. Reckamp, L. Goodglick and E. P. Diamandis, *Mol. Cell. Proteomics*, 2009, **8**, 2746–2758.

137 M. Infante, P. Allavena, C. Garlanda, M. Nebuloni, E. Morenghi, D. Rahal, M. Roncalli, S. Cavuto, S. Pesce, M. Monari, S. Valaperta, A. Montanelli, D. Solomon, E. Bottoni, V. Errico, E. Voulaz, M. Bossi, G. Chiesa, E. Passera, A. Mantovani and M. Alloisio, *Int. J. Cancer*, 2016, **138**, 983–991.

138 M. Locatelli, S. Ferrero, F. Martinelli Boneschi, L. Boiocchi, M. Zavanone, S. Maria Gaini, L. Bello, S. Valentino, E. Barbati, M. Nebuloni, A. Mantovani and C. Garlanda, *J. Neuroimmunol.*, 2013, **260**, 99–106.

139 F. Willeke, A. Assad, P. Findeisen, E. Schromm, R. Grobholz, B. von Gerstenbergk, A. Mantovani, S. Peri, H. H. Friess, S. Post, M. von Knebel Doeberitz and M. H. M. Schwarzbach, *Eur. J. Cancer*, 2006, **42**, 2639–2646.

140 T. H. Ying, C. H. Lee, H. L. Chiou, S. F. Yang, C. L. Lin, C. H. Hung, J. P. Tsai and Y. H. Hsieh, *Sci. Rep.*, 2016, **6**, 1–12.

141 D. Okutani, *Nihon Rinsho Meneki. Gakkai Kaishi*, 2006, **29**, 107–113.

142 S. Goodison, M. Chang, Y. Dai, V. Urquidi and C. J. Rosser, *PLoS One*, 2012, **7**, 6–11.

143 C. D. Yeo, J. W. Kim, M. R. Cho, J. Y. Kang, S. J. Kim, Y. K. Kim, S. H. Lee, C. K. Park, S. H. Kim, M. S. Park, H. W. Yim and J. Y. Park, *Tuberc. Respir. Dis. (Seoul).*, 2013, **75**, 244–249.

144 E. R. Zanier, G. Brandi, G. Peri, L. Longhi, T. Zoerle, M. Tettamanti, C. Garlanda, A. Sigurtà, S. Valaperta, A. Mantovani, M. G. De Simoni and N. Stocchetti, *Intensive Care Med.*, 2011, **37**, 302–309.

145 S. Padeh, N. Farzam, G. Chayen, M. Gerstein and Y. Berkun, *Immunol. Res.*, 2013, **56**, 444–450.

146 L. Cruciani, R. Romero, E. Vaisbuch, J. P. Kusanovic, T. Chaiworapongsa, S. Mazaki-Tovi, P. Mittal, G. Ogge, F. Gotsch, O. Erez, S. K. Kim, Z. Dong, P. Pacora, R. F. Lamont, L. Yeo, S. S. Hassan and G. C. Di Renzo, *J. Perinat. Med.*, 2010, **38**, 161–171.

147 F. E. Ahmed, *Expert Rev. Proteomics*, 2008, **5**, 841–864.

148 R. S. Tirumalai, K. C. Chan, D. R. A. Prieto, H. J. Issaq, T. P. Conrads and T. D. Veenstra, *Mol. Cell. Proteomics*, 2003, **2**, 1096–1103.

149 P. L. Kole, G. Venkatesh, J. Kotecha and R. Sheshala, *Biomed. Chromatogr.*, 2011, **25**, 199–217.

150 P. B. Kyle, in *Mass Spectrometry for the Clinical Laboratory*, Elsevier Inc., 2017, pp. 131–163.

151 G. Bahrami, S. Mirzaeei and A. Kiani, *J. Chromatogr. B Anal. Technol. Biomed. Life Sci.*, 2005,

816, 327–331.

152 R. Urkude, V. Dhurvey and S. Kochhar, in *Quality Control in the Beverage Industry*, Elsevier Inc., 2019, vol. 1, pp. 529–560.

153 D. A. Wells, *Solid-Phase Extraction with Cartridges*, Elsevier Inc., 2013.

154 S. Garcia, P. A. Baldasso, P. C. Guest and D. Martins-de-Souza, *Methods Mol. Biol.*, 2017, **1546**, 317 pp.

155 C. Wu, J. Duan, T. Liu, R. D. Smith and W. J. Qian, *J. Chromatogr. B Anal. Technol. Biomed. Life Sci.*, 2016, **1021**, 57–68.

156 W. J. Qian, D. T. Kaleta, B. O. Petritis, H. Jiang, T. Liu, X. Zhang, H. M. Mottaz, S. M. Varnum, D. G. Camp, L. Huang, X. Fang, W. W. Zhang and R. D. Smith, *Mol. Cell. Proteomics*, 2008, **7**, 1963–1973.

157 A. Rafalko, O. Iliopoulos, V. A. Fusaro, W. Hancock and M. Hincapie, *Anal. Chem.*, 2010, **82**, 8998–9005.

158 P. Y. Lee, J. Osman, T. Y. Low and R. Jamal, *Bioanalysis*, 2019, **11**, 1799–1812.

159 J. Stone, in *Mass Spectrometry for the Clinical Laboratory*, Elsevier Inc., 2017, pp. 37–62.

160 H. Mehrani, M. Ghanei, J. Aslani and Z. Tabatabaei, *Clin. Proteomics*, 2011, **8**, 2.

161 C. Bylda, R. Thiele, U. Kobold and D. A. Volmer, *Analyst*, 2014, **139**, 2265–2276.

162 J. F. B. Pereira, M. G. Freire and J. A. P. Coutinho, *Fluid Phase Equilib.*, 2020, **505**, 1–11.

163 F. F. Magalhães, A. P. M. Tavares and M. G. Freire, *Curr. Opin. Green Sustain. Chem.*, 2020, **27**, 100417.

164 R. R. G. Soares, A. M. Azevedo, J. M. Van Alstine and M. Raquel Aires-Barros, *Biotechnol. J.*, 2015, **10**, 1158–1169.

165 M. Van Berlo, K. C. A. M. Luyben and L. A. M. Van Der Wielen, *J. Chromatogr. B Biomed. Appl.*, 1998, **711**, 61–68.

166 Y. K. Yau, C. W. Ooi, E. P. Ng, J. C. W. Lan, T. C. Ling and P. L. Show, *Bioresour. Bioprocess.*, , DOI:10.1186/s40643-015-0078-0.

167 A. Karakatsanis and M. Liakopoulou-Kyriakides, *J. Food Eng.*, 2007, **80**, 1213–1217.

168 M. L. C. Neves, T. S. Porto, C. M. Souza-Motta, M. R. Spier, C. R. Soccol, K. A. Moreira and A. L. F. Porto, *Fluid Phase Equilib.*, 2012, **318**, 34–39.

169 I. A. O. Reis, S. B. Santos, L. A. Santos, N. Oliveira, M. G. Freire, J. F. B. Pereira, S. P. M. Ventura, J. A. P. Coutinho, C. M. F. Soares and Á. S. Lima, *Food Chem.*, 2012, **135**, 2453–2461.

170 F. Li, Y. Liu and W. Lin, *J. Mol. Liq.*, 2018, **256**, 372–379.

171 K. P. Ananthapadmanabhan and E. D. Goddard, *J. Colloid Interface Sci.*, 1986, **113**, 294–296.

172 A. M. Azevedo, A. G. Gomes, P. A. J. Rosa, I. F. Ferreira, A. M. M. O. Pisco and M. R. Aires-Barros, *Sep. Purif. Technol.*, 2009, **65**, 14–21.

173 L. P. Malpiedi, C. Fernández, G. Picó and B. Nerli, *J. Chem. Eng. Data*, 2008, **53**, 1175–1178.

174 A. Glyk, T. Scheper and S. Beutel, *Appl. Microbiol. Biotechnol.*, 2015, **99**, 6599–6616.

175 A. L. Grilo, M. R. Aires-Barros and A. M. Azevedo, *Sep. Purif. Rev.*, 2016, **45**, 68–80.

176 J. A. Asenjo and B. A. Andrews, *J. Chromatogr. A*, 2011, **1218**, 8826–8835.

177 M. G. Freire, A. F. M. Cláudio, J. M. M. Araújo, J. A. P. Coutinho, I. M. Marrucho, J. N. Canongia Lopes and L. P. N. Rebelo, *Chem. Soc. Rev.*, 2012, **41**, 4966–4995.

178 E. V Capela, J. H. P. M. Santos, I. Boal-palheiros, J. A. P. Coutinho, S. P. M. Ventura and M. G.

Freire, *Chem Eng Educ*, 2019, **53**, 112–120.

179 H. Tan and R. Lovrien, *J. Biol. Chem.*, 1972, **247**, 3278–3285.

180 C. Dennison and R. Lovrien, *Protein Expr. Purif.*, 1997, **11**, 149–161.

181 M. Gagaoua and K. Hafid, *Biosens. J.*, 2016, **5**, 1–4.

182 J. K. Yan, Y. Y. Wang, W. Y. Qiu, H. Ma, Z. Bin Wang and J. Y. Wu, *Crit. Rev. Food Sci. Nutr.*, 2018, **58**, 2416–2431.

183 M. Vargas, Á. Segura, M. Herrera, M. Villalta, Y. Angulo, J. M. Gutiérrez, G. León and T. Burnouf, *Biotechnol. Prog.*, 2012, **28**, 1005–1011.

184 E. V. Capela, A. E. Santiago, A. F. C. S. Rufino, A. P. M. Tavares, M. M. Pereira, A. Mohamadou, M. R. Aires-Barros, J. A. P. Coutinho, A. M. Azevedo and M. G. Freire, *Green Chem.*, 2019, **21**, 5671–5682.

185 F. D. Raymond, D. W. Moss and D. Fisher, *Clin. Chim. Acta*, 1994, **227**, 111–120.

186 N. Zhong, Y. Cui, X. Zhou, T. Li and J. Han, *Tumor Biol.*, 2015, **36**, 1221–1231.

187 M. Stovsky, L. Ponsky, S. Vourganti, P. Stuhldreher, M. B. Siroky, V. Kipnis, O. Fedotoff, L. Mikheeva, B. Zaslavsky, A. Chait and J. S. Jones, *Urology*, 2011, **78**, 601–605.

188 R. Y. T. Chiu, E. Jue, A. T. Yip, A. R. Berg, S. J. Wang, A. R. Kivnick, P. T. Nguyen and D. T. Kamei, *Lab Chip*, 2014, **14**, 3021–3028.

189 R. Y. T. Chiu, A. V. Thach, C. M. Wu, B. M. Wu and D. T. Kamei, *PLoS One*, 2015, **10**, 1–14.

190 J. P. Frampton, J. B. White, A. B. Simon, M. Tsuei, S. Paczesny and S. Takayama, *Sci. Rep.*, 2014, **4**, 14–16.

191 E. A. Klein, A. Chait, J. M. Hafron, K. M. Kernen, K. Manickam, A. J. Stephenson, M. Wagner, H. Zhu, A. Kestranek, B. Zaslavsky and M. Stovsky, *Eur. Urol.*, 2017, **72**, 942–949.

192 J. F. B. Pereira, L. P. N. Rebelo, R. D. Rogers, J. A. P. Coutinho and M. G. Freire, *Phys. Chem. Chem. Phys.*, 2013, **15**, 19580–19583.

193 D. W. Bradbury, M. Azimi, A. J. Diaz, A. A. Pan, C. H. Falktoft, B. M. Wu and D. T. Kamei, *Anal. Chem.*, 2019, **91**, 12046–12054.

194 B. Y. Zaslavsky, V. N. Uversky and A. Chait, *Biochim. Biophys. Acta - Proteins Proteomics*, 2016, **1864**, 622–644.

195 J. C. Merchuk, B. A. Andrews and J. A. Asenjo, *J. Chromatogr. B Anal. Technol. Biomed. Life Sci.*, 1998, **711**, 285–293.

196 L. M. Pegram and M. T. Record, *J. Phys. Chem. B*, 2007, **111**, 5411–5417.

197 K. P. Ananthapadmanabhan and E. D. Goddard, *Langmuir*, 1987, **3**, 25–31.

198 M. T. Zafarani-Moattar, S. Hamzehzadeh and S. Nasiri, *Biotechnol. Prog.*, 2012, **28**, 146–156.

199 H. Passos, A. C. A. Sousa, M. R. Pastorinho, A. J. A. Nogueira, L. P. N. Rebelo, J. A. P. Coutinho and M. G. Freire, *Anal. Methods*, 2012, **4**, 2664–2667.

200 S. P. M. Ventura, S. G. Sousa, L. S. Serafim, Á. S. Lima, M. G. Freire and J. A. P. Coutinho, *J. Chem. Eng. Data*, 2012, **57**, 507–512.

201 Y. Pei, J. Wang, K. Wu, X. Xuan and X. Lu, *Sep. Purif. Technol.*, 2009, **64**, 288–295.

202 I. M. Vlasova and A. M. Saletsky, *J. Appl. Spectrosc.*, 2009, **76**, 536–541.

203 F. Chiodi, Å. Sidén and E. Ösby, *Electrophoresis*, 1985, **6**, 124–128.

204 R. Pieper, C. L. Gatlin, A. J. Makusky, P. S. Russo, C. R. Schatz, S. S. Miller, Q. Su, A. M. McGrath, M. A. Estock, P. P. Parmar, M. Zhao, S. T. Huang, J. Zhou, F. Wang, R. Esquer-Blasco,

N. L. Anderson, J. Taylor and S. Steiner, *Proteomics*, 2003, **3**, 1345–1364.

VI– APPENDIX

Table A1. Experimental weight fraction data obtained for the systems composed of PPG 400, PEG 400 or PEG 600 (1) + $K_3C_6H_5O_7/C_6H_8O$ (2) + H_2O (3).

PPG 400		**PEG 400**		**PEG 600**	
$100w_1$	$100w_2$	$100w_1$	$100w_2$	$100w_1$	$100w_2$
67.8727	1.2429	40.9489	13.1914	56.0926	2.8514
47.1949	2.1737	38.0336	14.3724	52.8435	4.3331
43.3354	2.9428	35.8680	15.6539	49.0415	6.4270
39.5914	3.6991	34.1796	16.3385	47.0423	7.4788
36.3995	4.9461	31.2147	18.1117	44.4806	8.6450
33.1945	5.3280	28.8854	19.3821	41.5768	10.3288
31.2503	5.7009	26.3010	21.1923	40.2221	11.0471
29.8439	6.1647	24.2170	22.5810	38.0314	12.3418
28.8037	6.6311	22.1192	24.1541	36.3307	13.2015
27.3859	7.1425	21.6064	24.4753	34.9962	14.0934
25.8121	7.2852	19.9751	25.6467	33.3315	15.0149
24.8240	7.5935	18.8788	26.4737	31.7541	15.9648
24.2248	7.6740	17.2551	27.5930	30.6188	16.5936
23.6340	7.7639	16.2796	28.2426	30.0180	16.8633
23.2264	7.9555	15.1659	29.1232	29.3283	17.2474
22.6060	8.6242	14.3251	29.7564	28.7339	17.5933
21.5631	8.5016	13.5690	30.2693	27.6961	18.1529
21.2780	8.6061	12.9328	30.7678	26.0080	19.0864
20.8079	8.6425	12.3906	31.1505	25.1411	19.5187
20.1020	9.1929	11.8510	31.5550	24.3361	20.0107
19.2673	9.2175	11.1105	32.2367	23.4012	20.6474
18.7233	9.2378	10.6794	32.5120	22.5786	21.0603
18.0110	9.7059	10.1919	32.8858	22.0543	21.3139
17.3676	9.7965	9.7641	33.3139	21.3950	21.6172
16.8447	9.8871	9.3878	33.6427	20.7884	22.0122
16.3669	9.9858			20.5806	21.9921
16.0685	10.0813			20.2370	22.1196
15.6590	10.2382			19.8207	22.4235
15.4137	10.4103			19.4123	22.7519
14.5397	10.4252			19.1088	22.9066
14.2177	10.6676			18.5378	23.2335
13.7698	10.7815			18.1254	23.4165
13.2969	10.7174			17.7759	23.6701
12.9246	10.9839			17.3416	23.9172
12.5087	11.1050			17.0534	24.0304
12.0531	11.3142			16.5456	24.3582
11.6000	11.3885			16.1400	24.5947
11.1893	11.6179			15.8603	24.7140
10.8691	11.9383			15.5965	24.8964
10.4515	11.9277			15.2934	25.0093
10.1149	12.1076			15.1360	25.1230
9.8278	12.3407			14.7835	25.3637
9.3660	12.6613			14.3133	25.7781
9.0887	12.6293			13.8961	25.9964
8.8669	12.7055			13.6621	26.1182

8.6247	12.8741			13.3645	26.2362
8.4637	13.0025			13.0829	26.4428
8.2418	13.0389			12.7494	26.5655
8.0688	13.2259			12.5903	26.6416
7.7847	13.3315			12.3480	26.7836
7.6143	13.4732			12.0430	26.9741
7.4703	13.5920			11.8109	27.0977
7.2714	13.6840			11.5396	27.3186
7.0565	13.8186			11.5396	27.3186
6.8901	13.8555				
6.7521	13.8988				
6.5858	14.0814				
6.4123	14.2522				
6.2571	14.2332				
6.1614	14.4555				
5.9632	14.5760				
5.7300	14.7097				
5.5824	14.8656				
5.4630	14.9421				
5.2772	15.0612				
5.1752	15.1410				
5.0497	15.1518				

Table A2. Experimental weight fraction data obtained for the systems composed of PEG 1000, PEG 2000 or UCON (1) + $K_3C_6H_5O_7/C_6H_8O$ (2) + H_2O (3).

PEG 1000		**PEG 2000**		**UCON**	
$100w_1$	$100w_2$	$100w_1$	$100w_2$	$100w_1$	$100w_2$
52.8512	4.7549	50.4483	2.5485	25.2632	6.9751
40.6825	7.2844	45.6759	5.1833	23.8550	7.2867
35.0029	9.1476	40.8259	5.8473	22.8016	7.7010
31.9093	10.0963	37.3859	6.7536	21.8898	8.1636
29.4974	10.7474	34.9246	7.4240	20.6271	8.4623
27.4443	11.7919	31.9705	7.8865	19.9111	8.8953
25.6119	12.8311	30.2289	8.5393	18.6683	9.4303
24.1836	13.5054	28.6906	9.0973	17.4520	9.4925
22.9218	14.1859	27.1338	9.6827	16.8577	9.7708
22.0746	14.7836	25.4836	10.0948	16.3773	10.0184
21.0402	15.2411	24.6278	10.5958	15.8420	10.2461
19.9626	15.8458	23.5453	10.7258	15.4170	10.3763
18.9284	16.5824	23.0125	11.0188	14.8854	10.6729
18.0506	17.0675	22.2407	11.2406	14.4418	10.8047
17.2126	17.5702	21.7844	11.4960	14.0581	10.9326
16.6079	17.9526	21.3299	11.7285	13.7388	11.1813
15.9651	18.2763	20.6914	11.7905	13.1723	11.5408
15.5722	18.6540	20.2693	12.0497	12.7156	11.6791
15.1045	19.1420	19.8248	12.2437	12.2364	12.0527
14.4459	19.6417	19.4157	12.4037	11.8325	12.3324

13.8022	19.8049	18.9161	12.7894	11.2790	12.5845
13.4374	19.8375	18.4303	13.2162	10.7824	12.6951
12.9870	20.1051	17.8718	13.3372	10.5035	12.8317
12.5170	20.4966	17.5703	13.4871	10.1550	13.1408
12.1700	20.6550	17.2734	13.7255	9.8213	13.3541
11.8031	20.8703	16.9965	13.8626	9.4346	13.3640
11.4138	21.0672	16.7106	13.9658	9.1436	13.6237
11.1064	21.2396	16.4598	14.1274	8.7763	13.7000
10.7819	21.4352	16.1824	14.3262	8.4971	13.7412
10.5090	21.8257	15.8335	14.7595	8.0585	13.5939
10.0782	22.0628	15.3515	14.8549	7.8835	13.7349
9.8399	22.1326	15.0052	14.8485	7.6458	13.7462
9.5884	22.2813	14.6418	15.1990	7.4729	13.8850
9.3120	22.5178	14.3716	15.1416	7.3371	14.0564
9.0126	22.8572	14.1751	15.2484	7.1164	14.1289
8.8323	22.9203	13.9994	15.3321	6.9485	14.2655
8.6239	23.0737	13.7910	15.4929	6.7084	14.2264
8.3787	23.1367	13.6497	15.6331	6.5947	14.4260
8.1319	23.4212	13.3970	15.7443	6.4119	14.2976
7.8713	23.5771	13.1953	15.8688	6.3188	14.5493
7.6334	23.7248	12.8380	15.9766	6.1588	14.6543
7.3832	23.9560	12.5096	16.2080	6.0029	14.6388
7.1681	24.0826	12.2535	16.3902	5.8704	14.6833
6.9642	24.2152	12.0312	16.3865	5.7521	14.9146
6.7922	24.4418	11.6083	16.8108	5.6160	14.8906
6.6137	24.5765	11.2875	17.0049	5.4990	14.9525
6.4267	24.6975	11.0063	17.0759	5.3791	14.9912
6.2429	24.9147	10.7809	17.2411	5.2889	14.9687
6.0730	25.0456	10.5734	17.3989	5.1860	15.0090
5.9636	25.0820	10.3344	17.5552	5.0760	15.1015
5.8244	25.3248	10.1015	17.7729	4.9671	15.0860
5.6998	25.3588	9.8183	17.9960	4.8825	15.3377
5.5704	25.4780	9.5251	18.0906	4.6923	15.4868
5.4216	25.6444	9.1503	18.4446	4.5540	15.5469
5.2491	25.7901	8.9302	18.3134	4.4055	15.6211
5.0853	25.9495	8.6942	18.5378	4.2943	15.6641
4.9866	25.9946	8.4552	18.5331	4.2075	15.8237
		8.2313	18.7535	4.0673	15.8911
		7.9054	18.9345	3.9312	15.9702
		7.7801	19.0097	3.8281	16.1608
		7.6065	19.1420	3.6955	16.3144
		7.4310	19.3065	3.5992	16.4034
		7.2254	19.3831		
		7.0546	19.2857		
		6.8662	19.5970		
		6.7148	19.5732		
		6.5530	19.8620		
		6.3817	19.8427		
		6.2441	20.0588		
		6.0888	20.0598		

		5.9662	20.1695		
		5.8377	20.2929		
		5.6607	20.3904		
		5.4720	20.7828		
		5.2604	20.6424		

Table A3. Experimental weight fraction data obtained for the systems composed of Pluronic PE6200, Pluronic PE6400 or Pluronic L35 (1) + $K_3C_6H_5O_7$/C_6H_8O (2) + H_2O (3).

Pluronic PE6200		**Pluronic PE6400**		**Pluronic L35**	
$100w_1$	$100w_2$	$100w_1$	$100w_2$	$100w_1$	$100w_2$
51.8470	3.2731	51.2535	2.9827	24.2378	9.2837
45.9415	5.6115	45.6493	3.9150	23.1770	9.4248
36.9204	5.4504	40.0043	4.9957	21.8527	9.2163
33.5061	5.9585	37.8505	5.3164	21.0684	9.4542
30.9379	6.0138	35.8035	5.8247	20.3016	9.4950
29.2835	6.5819	33.3134	7.0143	19.6752	9.6572
27.2384	6.9975	29.2730	6.9680	18.9644	9.8294
24.6507	7.1551	28.0363	7.5372	18.1977	10.0372
22.9698	7.3953	25.7156	8.6484	17.4472	9.7410
21.1106	7.7523	23.2347	8.5644	17.1858	10.0424
19.9806	7.9094	22.0360	8.6894	16.6538	10.0793
18.8906	8.0536	21.4379	8.8213	16.0044	10.3626
18.3390	8.3306	20.8527	9.0751	15.5501	10.5206
17.6282	8.6792	19.9276	9.6560	15.1647	10.5839
16.7531	8.6664	18.6868	9.6010	14.8038	10.7149
15.9214	8.7994	18.0277	9.8098	14.3814	11.0146
15.0865	8.8584	17.2825	9.8989	13.8710	11.0114
14.0887	8.8548	16.6532	10.3137	13.4772	11.0864
13.3873	8.7398	15.8700	10.5564	13.0882	11.2396
12.8777	8.7172	15.0966	10.4568	12.6004	11.1607
12.5135	8.7599	14.6165	10.5592	12.3125	11.4458
12.1476	8.8335	14.2539	10.6128	11.9219	11.5635
11.7119	8.8961	13.9401	10.7891	11.5996	11.5155
11.3355	8.9010	13.4217	10.8893	11.1274	11.8727
10.9450	8.9710	12.9416	11.0616	10.7085	11.7165
10.5211	8.9433	12.5960	11.0837	10.4665	11.6972
10.1488	8.9662	12.3047	11.1203	10.2286	11.7173
9.7068	8.8553	12.0199	11.2079	9.9993	11.6796
9.4170	8.8738	11.7108	11.3952	9.8771	11.6891
9.1326	8.8425	11.4283	11.3823	9.7543	11.7726
8.8707	8.8584	11.1590	11.4745	9.5423	11.9690
8.6036	8.9307	10.9335	11.4693	9.2991	11.9001
8.3143	9.0577	10.6719	11.6123	9.0986	11.8744
8.1908	9.0988	10.3599	11.7706	8.9049	12.0923
8.0568	9.1525	10.1376	11.8951	8.6267	12.0472
7.9008	9.1697	9.8619	11.9340	8.4889	11.9543
7.7384	9.1553	9.6381	11.9880	8.4109	12.0539
7.5699	9.2483	9.4696	12.0850	8.3265	12.0908

7.3597	9.1326	9.3048	12.0131	8.1982	12.1904
7.1622	9.1584	9.1948	12.1439	7.9820	12.2113
6.9530	9.1119	9.0295	12.1982	7.7337	12.2602
6.7246	8.9851	8.8725	12.2182	7.5371	12.2342
		8.7281	12.2500	7.4388	12.2157
		8.5885	12.2429	7.2722	12.1769
		8.4231	12.4190	7.1537	12.2417
		8.2108	12.4689	7.0501	12.2264
		8.0029	12.4985	6.9484	12.2554
		7.8218	12.5107	6.8657	12.2673
		7.7235	12.4467	6.7634	12.3552
		7.5860	12.6162	6.5937	12.5525
		7.4385	12.6201	6.4601	12.4445
		7.3197	12.6057	6.3721	12.4840
		7.1952	12.5278	6.2343	12.3652
		7.0916	12.6900	6.1329	12.6135
		6.9821	12.7702	5.9213	12.4266
		6.8585	12.7051	5.8655	12.5704
		6.7748	12.7729	5.7446	12.6057
		6.6431	12.7810	5.6077	13.0009
		6.5242	12.7562	5.5094	13.0217
		6.4303	12.8500	5.4422	13.1295
		6.3274	12.8615	5.3080	13.0787
		6.2410	12.9145		
		6.1713	12.8826		
		6.1038	12.9208		
		6.0396	12.9350		
		5.9665	12.9360		
		5.8863	12.9982		
		5.8219	12.9960		

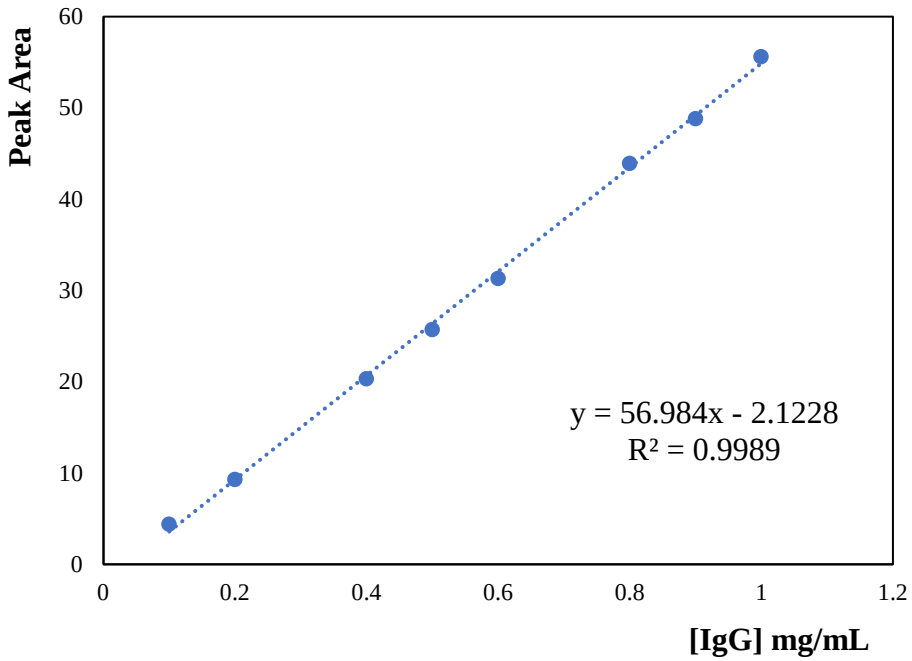

Figure A1. Calibration curve for IgG by SE-HPLC.

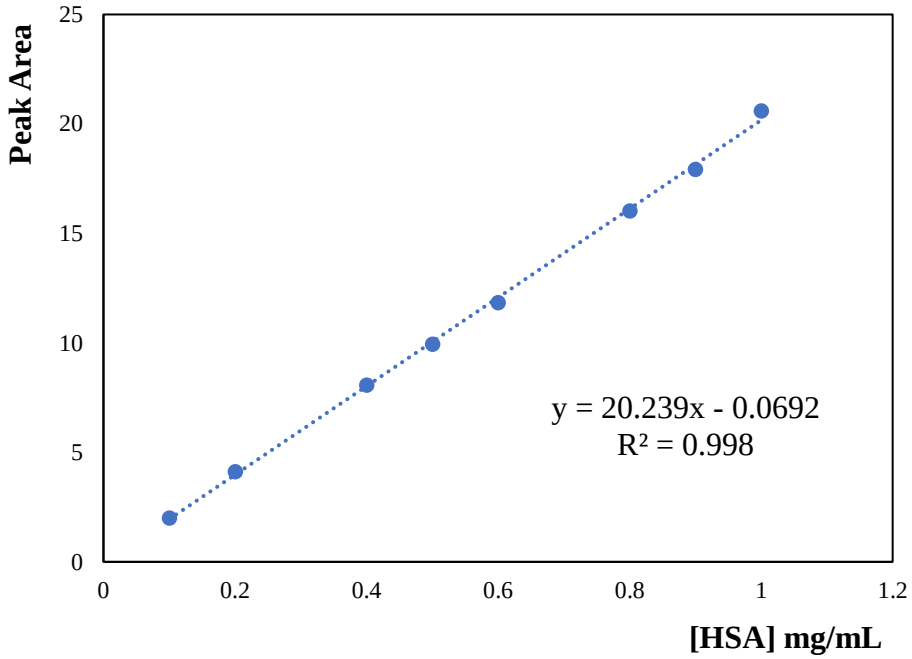

Figure A2. Calibration curve for HSA by SE-HPLC.

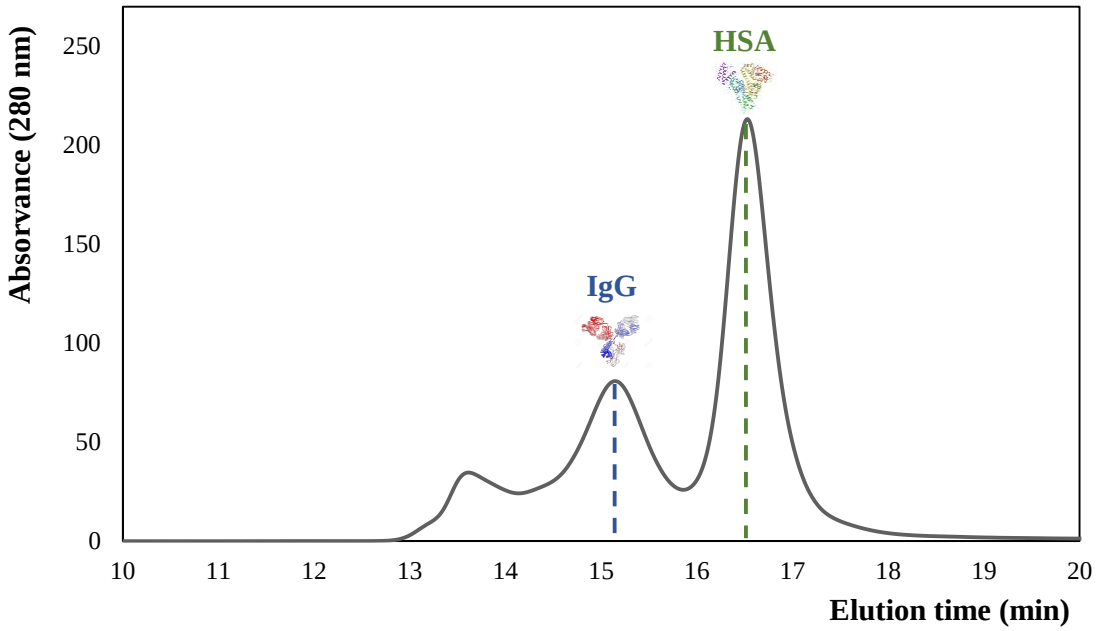

Figure A3. SE-HPLC chromatogram of the human serum sample diluted in aqueous solution. The blue line corresponds to the retention time of IgG and the green line to the retention time of HSA.

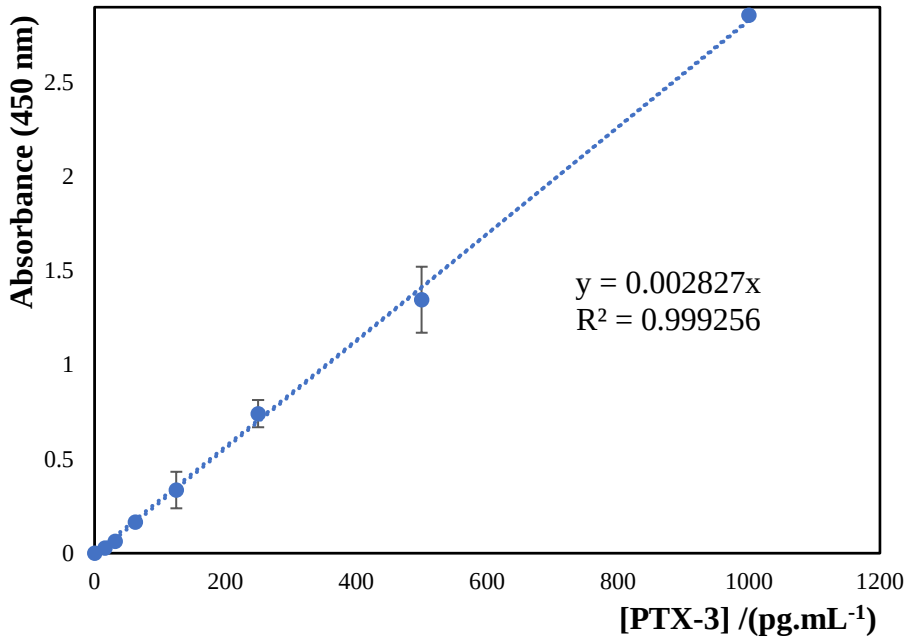

Figure A4. Calibration curve for PTX-3 by ELISA.

Table A4. Comparison between depletions efficiencies of systems formed by 30 wt% of homopolymer and 30 wt% of $K_3C_6H_5O_7/C_6H_8O_7$ with different protein compositions.

Polymer	Depletion efficiencies (%)					
	Serum		HSA + IgG		HSA	IgG
	HSA	IgG	HSA	IgG		
PPG 400	86.0862 ± 2.1545	87.7196 ± 0.1731	78.5715 ± 2,9812	82.9247 ± 0.1195	75.2002 ± 1.4922	80.1676 ± 5.2624
PEG 400	8.7768 ± 2.4657	29.0013 ± 0.2379	5.0649 ± 0.1489	21.7656 ± 1.0712	4.1339 ± 0.4377	15.7413 ± 0.6953
PEG 600	24.1791 ± 3.2757	51.9805 ± 1.3284	17.8816 ± 3.8707	37.9903 ± 3.6056	4.2560 ± 0.6851	29.9510 ± 0.7309
PEG 1000	94.7045 ± 1.0355	88.3926 ± 0.2379	63.9506 ± 1.2127	53.3946 ± 1.2864	56.9519 ± 0.1373	44.1842 ± 1.7192
PEG 2000	82.9267 ± 3.8390	82.3132 ± 2.3208	79.1189 ± 1.6821	54.7376 ± 3.9797	59.5195 ± 0.4465	45.7815 ± 0.9822

Table A5. Comparison between depletions efficiencies of systems formed by 30 wt% of copolymer and 30 wt% of $K_3C_6H_5O_7/C_6H_8O_7$ with different protein compositions.

Copolymer	Depletion efficiencies (%)					
	Serum		HSA + IgG		HSA	IgG
	HSA	IgG	HSA	IgG		
Pluronic PE6200	41.7223 ± 1.0355	39.8616 ± 0.2379	11.8243 ± 0.0482	31.8905 ± 1.7657	8.6356 ± 0.0608	27.1722 ± 0.4387
Pluronic PE6400	40.5265 ± 0.5932	32.1353 ± 3.8489	9.2988 ± 0.9335	26.2676 ± 0.3950	7.1162 ± 0.2767	25.9544 ± 2.6393
Pluronic L35	84.1007 ± 4.7519	68.9017 ± 2.9408	70.3077 ± 2.1539	65.4123 ± 2.9182	59.4067 ± 1.7453	50.3262 ± 1.1106
UCON	92.2704 ± 1.8473	81.3805 ± 1.5737	32.2707 ± 3.6878	44.6888 ± 2.8235	26.5133 ± 0.6741	34.6617 ± 1.6082

Table A6. Extraction efficiency of PTX-3 (EE_{PTX-3}%) at 25° C in the ABS composed of 30 wt% of homopolymer/copolymer and 30 wt% of $K_3C_6H_5O_7/C_6H_8O_7$, at 25ºC and atmospheric pressure.

Homopolymer/ Copolymer	EE_{PTX-3}%
PPG 400	100.0 ± 0.0000
PEG 1000	100.0 ± 0.0000
PEG 2000	100.0 ± 0.0000
UCON	100.0 ± 0.0000
Pluronic L35	100.0 ± 0.0000

Table A7. Mass percentage of PTX-3 in the top phase, interphase, and bottom phase in TPP formed by 30 wt% of homopolymer/copolymer and 30 wt% of $K_3C_6H_5O_7/C_6H_8O_7$, at 25ºC and atmospheric pressure.

Homopolymer/ Copolymer	Mass percentage of PTX-3 / %		
	Top phase	Interphase	Bottom phase
PPG 400	0.2096 ± 0.2964	94.3817 ± 1.5476	5.4087 ± 1.2512
PEG 1000	99.7552 ± 0.3462	0.2448 ± 0.2448	0.0000 ± 0.0000
PEG 2000	0.0000 ± 0.0000	94.2118 ± 4.6394	5.7882 ± 4.6394
UCON	54.3393 ± 12.1011	51.5440 ± 12.1011	0.0000 ± 0.0000
Pluronic L35	48.4560 ± 13.5642	45.6607 ± 13.5642	0.0000 ± 0.0000